Research Square

Preprints are preliminary reports that have not undergone peer review.
They should not be considered conclusive, used to inform clinical practice,
or referenced by the media as validated information.

Plasma and CSF neurofilament light chain are stabilized in response to mutant huntingtin lowering in the brain of Huntington disease mice

Nicholas S. Caron
The University of British Columbia Centre for Molecular Medicine and Therapeutics
Lauren M. Byrne
University College London Queen Square Institute of Neurology
Fanny L. Lemarié
The University of British Columbia Centre for Molecular Medicine and Therapeutics
Jeffrey N. Bone
BC Children's Hospital Research Institute
Amirah E.-E. Aly
The University of British Columbia Centre for Molecular Medicine and Therapeutics
Seunghyun Ko
The University of British Columbia Centre for Molecular Medicine and Therapeutics
Christine Anderson
The University of British Columbia Centre for Molecular Medicine and Therapeutics
Lorenzo Casal
The University of British Columbia Centre for Molecular Medicine and Therapeutics
Austin M. Hill
The University of British Columbia Centre for Molecular Medicine and Therapeutics
David J. Hawellek
Hoffmann-La Roche: Hoffmann-La Roche Limited
Peter McColgan
Roche Products Ltd: Roche UK Ltd
Edward J. Wild
University College London Queen Square Institute of Neurology
Blair R. Leavitt
The University of British Columbia Centre for Molecular Medicine and Therapeutics
Michael R Hayden
mrh@cmmt.ubc.ca

The University of British Columbia

Research Article

Keywords: Neurofilament light chain, response biomarker, Huntington disease, huntingtin lowering, antisense oligonucleotide, cerebrospinal fluid, plasma, biofluids

Posted Date: May 22nd, 2024

DOI: https://doi.org/10.21203/rs.3.rs-4378780/v1

License: This work is licensed under a Creative Commons Attribution 4.0 International License.
Read Full License

Version of Record: A version of this preprint was published at Translational Neurodegeneration on October 8th, 2024. See the published version at https://doi.org/10.1186/s40035-024-00443-8.

Abstract

Background

Therapeutic approaches aimed at lowering levels of toxic mutant huntingtin (mHTT) in the brain can reverse disease phenotypes in animal models of Huntington disease (HD) and are currently being evaluated in clinical trials. Sensitive and dynamic response biomarkers are needed to assess the efficacy of such candidate therapies. Neurofilament light chain (NfL) is a biomarker of neurodegeneration that increases in cerebrospinal fluid (CSF) and blood with HD progression. However, it remains unknown whether NfL in biofluids may be useful as a response biomarker for assessing the efficacy of disease-modifying therapies for HD.

Methods

Longitudinal plasma and cross-sectional CSF samples were collected from the YAC128 transgenic mouse model of HD and wild type littermate control mice throughout the natural history of disease. Additionally, biofluids were collected from YAC128 mice following intracerebroventricular administration of an antisense oligonucleotide targeting the mutant *HTT* transgene (HTT ASO) at ages either before or after the onset of disease phenotypes. NfL concentrations in plasma and CSF were quantified using ultrasensitive single-molecule array technology.

Results

Plasma and CSF NfL concentrations were significantly elevated in YAC128 compared to wild type littermate control mice from 9 months of age. Treatment of YAC128 mice with either 15 or 50 µg HTT ASO resulted in dose-dependent, allele-selective reduction of mHTT throughout the brain at a 3-month interval, which was sustained with high dose HTT ASO treatment up 6 months. Lowering of mHTT in the brain with HTT ASO initiated prior to the onset of regional brain atrophy and HD-like motor deficits in YAC128 mice had minimal effect on plasma NfL at either dose but resulted in a dose-dependent reduction of CSF NfL. In contrast, initiating mHTT lowering in the brain after the onset of neuropathological and behavioural phenotypes in YAC128 mice resulted in a dose-dependent stabilization of NfL increases in both plasma and CSF.

Conclusions

Our data provides evidence that the response of NfL in biofluids is influenced by the magnitude of mHTT lowering in the brain and the timing of intervention, suggesting that NfL may represent a promising exploratory response biomarker for HD.

Background

Huntington disease (HD) is a fatal neurodegenerative disorder for which there is no effective disease-modifying treatment. HD is caused by a CAG repeat expansion mutation in the *HTT* gene that codes for an abnormal polyglutamine tract in the huntingtin (HTT) protein (1). Polyglutamine-expanded mutant HTT (mHTT) disrupts multiple cellular processes and pathways (reviewed in (2)) leading to progressive degeneration of selected neuronal populations in the basal ganglia and cerebral cortex (3–11).

Targeting a proximal cause of HD pathogenesis by lowering levels of mHTT in the central nervous system (CNS) has emerged as a promising therapeutic approach for HD. Preclinical studies in HD rodent models have demonstrated that pharmacological mHTT lowering in the CNS can prevent HD-like behavioural deficits and progressive neurological phenotypes, including regional forebrain atrophy and neurodegeneration (12–14). These findings have accelerated clinical development of multiple HTT lowering modalities and have led to the therapeutic trials evaluating antisense oligonucleotides (ASOs) (15–20), RNA interference-based (21, 22) and small molecules (23, 24) for HD.

HD typically presents in the clinic as an adult-onset disease that manifests as a spectrum of movement, cognitive and psychiatric disorders, where symptom heterogeneity is associated with the magnitude and regional patterns of striatal and cortical neurodegeneration (25–29). Clinical diagnosis is made based on the presence of unequivocal motor signs of HD. However, many HD mutation carriers experience cognitive decline and psychiatric symptoms prior to clinical diagnosis, during the premanifest or prodromal stage of disease. Neuroimaging studies in premanifest HD mutation carriers have revealed striatal volume loss up to 20 years prior to predicted symptomatic manifestation (30–38), which suggests that pathogenic molecular processes and cellular dysfunction are occurring in the brain many years before clinical onset. Therefore, therapies aimed at modifying the course of the disease may be most effective if intervention is initiated early, prior to profound neurodegeneration and functional decline. However, there remains an unmet need to identify sensitive and objective biomarkers that change in a predictable manner in response to intervention to provide evidence of therapeutic efficacy.

Molecular biomarkers in biological fluids (ie. biofluids) offer the potential to non-invasively and objectively monitor pathophysiological alterations in the CNS associated with HD. Sensitive and dynamic molecular biomarkers that reflect altered neuronal health, neurodegeneration or other underlying pathogenic processes could be used to detect early pathological changes in premanifest disease. They may also be useful to complement existing clinical measures and/or imaging biomarkers for monitoring disease progression and assessing therapeutic efficacy of candidate therapies in clinical trials for HD.

Multiple protein biomarkers have been identified in CSF and/or blood that are altered in HD mutation carriers and correlate with clinical measures of disease, including mHTT (39–42), neurofilament light chain (NfL) (41–46), proenkephalin (46, 47), prodynorphin (46, 48), microtubule-associated protein tau (49–51), and YKL-40 (chitinase-3-like protein 1) (52, 53). Moreover, we recently defined specific combinations of CSF biomarkers that could be used to reliably stratify individuals based on HD severity (46).

Neurofilaments are a family of neuron-specific intermediate filaments that are key structural components of the axonal cytoskeleton. NfL is released from neurons as a result of neuroaxonal damage and can be measured in the CSF and blood (54). Elevated concentrations of NfL in biofluids, indicating neuronal injury and/or neurodegeneration, have been reported in several neurological disorders, including HD (38, 41–45), multiple types of spinocerebellar ataxia (55), spinal muscular atrophy (SMA) type 1 (56), amyotrophic lateral sclerosis (ALS) (57, 58), Parkinson disease (59, 60), and Alzheimer disease (61, 62). Increased biofluid NfL concentrations have also been reported in multiple sclerosis (MS) (63–68), traumatic brain injury (69–71) and CNS infection (72).

In HD, concentrations of NfL in CSF and blood increase with disease severity and are associated with clinical measures of cognitive and motor function as well as imaging measures of regional brain atrophy (41, 43). Moreover, NfL levels in biofluids are a strong prognostic biomarker of disease onset, clinical progression and brain atrophy in HD patients (42, 43, 45). Notably, elevated CSF and plasma NfL are one of the earliest measurable pathological alterations in HD (41), with significant increases reported in premanifest HD mutation carriers approximately 24 years before predicted disease onset (38). These findings suggest that increased NfL levels in blood and CSF reflect early perturbations to neuronal health in the brain that may precede atrophy, degeneration and subsequent cell loss. Consistent with data from HD mutation carriers, elevated NfL concentrations in biofluids have been reported in both transgenic (eg. YAC128) and knock-in (eg. zQ175) mouse models of HD (73–75).

Biofluid NfL concentrations have also been adopted as a response biomarker for evaluating candidate therapies in clinical trials for multiple neurological disorders, including HD. Evidence from trials in relapsing-remitting MS and progressive MS have shown that some therapies that effectively reduce axonal damage can lead to decreased NfL levels in both serum and CSF (76–81). Studies in children with SMA type 1 treated with nusinersen, an ASO that modulates the splicing of the *SMN2* gene, showed a decrease in CSF NfL that was associated with improved motor function (56, 82). Recently, a phase III trial in ALS patients with *SOD1* mutations showed that treatment with the superoxide dismutase 1-lowering ASO, tofersen, led to a reduction of plasma NfL but did not significantly improve clinical measures of disease (83). Plasma NfL in this trial was accepted as a surrogate efficacy endpoint by the FDA based on the reasonable likelihood that its reduction would predict clinical benefit and led to tofersen being granted accelerated approval for treatment of *SOD1* ALS.

CSF and/or blood NfL concentrations have been used as an exploratory endpoint of HD progression and therapeutic response in trials for HTT lowering therapies (21, 84–86). Preliminary results from the phase III GENERATION HD1 trial evaluating the efficacy of an ASO targeting the *HTT* transcript for degradation, tominersen (RO7234292), showed that CSF NfL concentrations were trending below baseline levels in response to sustained mHTT lowering in the CNS of individuals undergoing less frequent dosing (every 16 weeks) (86). However, no improvements were seen overall in clinical or exploratory imaging outcome measures in response to tominersen treatment (86). Additional studies evaluating the relationship between NfL levels in biofluids and mHTT lowering in the brain are needed for the accurate interpretation of clinical NfL data.

In this study, we sought to investigate whether NfL concentrations in biofluids are responsive to allele-selective lowering of mHTT in the brain, and if the magnitude of mHTT lowering in the brain or timing of intervention during the disease influences this response. We hypothesized that NfL concentrations in CSF and blood, which increase with disease progression in HD, would be stabilized or decrease in response to mHTT lowering in the brain. To test this, we utilized the well-characterized transgenic YAC128 mouse model of HD that expresses human, full-length mHTT and recapitulates many of the neuropathological, behavioural and biochemical features of the human disease (87). YAC128 mice develop progressive striatal atrophy starting at 3 months (88, 89), motor deficits as early as 4 months (90–92), and selective striatal neuron loss from 9–12 months of age (87, 93), thus providing a opportunities to explore the relationship of mHTT lowering in the brain - initiated either prior or subsequent to the onset HD-like motor deficits and neurodegeneration - on NfL concentrations in biofluids. We used single molecule array (SIMOA) for ultrasensitive measurement of NfL in cross-sectional CSF and longitudinal plasma samples from YAC128 and wild type (WT) littermate control mice.

After characterizing the natural history of NfL in the CSF and plasma of YAC128 and WT littermate control mice up to 15 months of age, we assessed CSF and plasma NfL concentrations over a 3-month interval in response to mHTT lowering in the CNS of YAC128 mice with either 15 µg (low dose) or 50 µg (high dose) of ASO targeting the human mutant *HTT* transcript (HTT ASO) initiated at either 2 or 12 months of age. We then assessed biofluid NfL concentrations over a 6-month interval in response to mHTT lowering in the CNS of YAC128 with high dose HTT ASO initiated at 8 months of age. These studies were designed to evaluate the response of NfL in biofluids to mHTT lowering in the brain initiated at different ages in YAC128 mice to model therapeutic intervention during the premanifest (pre-symptomatic) and manifest (symptomatic) stages of HD.

Methods

Study design

The primary objectives of this study were to investigate whether NfL concentrations in plasma and CSF respond to mHTT lowering in the brain, and whether the magnitude and timing of mHTT lowering may influence this response. We utilized the YAC128 mouse model of HD that exhibits neuropathological, behavioural and biochemical features similar to those observed in HD patients. NfL concentrations in CSF and plasma over the natural history of disease in YAC128 and WT littermate control mice were characterized to assess whether YAC128 mice accurately model elevated NfL concentrations observed in HD mutation carriers (Fig. 1). We evaluated NfL concentrations in biofluids following intraparenchymal injections of quinolinic acid (QA) to the striatum to elucidate the dynamics of NfL changes in CSF and plasma in response to acute neurotoxicity in the brain (Fig. 2). Intracerebroventricular (ICV) injections with a HTT ASO was used to lower mHTT in the CNS of YAC128 mice (Fig. 3). Dosing was informed by previous studies using the same HTT ASO with the goal of achieving ~ 50% mHTT reduction and ~ 75% mHTT reduction in the brain at a 1-month treatment interval with the low (15 µg HTT ASO) and high dose (50 µg HTT ASO), respectively. Timing of mHTT lowering intervention in YAC128 mice were carefully

selected based on extensive phenotypic characterization of this line. The early intervention timepoint (2 months of age) was selected to be an age where YAC128 are developed adults but before reported motor deficits and neuropathological phenotypes, to model therapeutic intervention during premanifest HD. The late intervention timepoint (12 months of age) was selected to be an age where YAC128 mice display robust regional forebrain atrophy and selective striatal neuron loss to model intervention at a more advanced stage of disease. Finally, the mid intervention timepoint (8 months of age) was selected to be at an age when clear phenotypes in YAC128 are present, but are still progressing, in order to model intervention in an early/mid stage of HD. We evaluated CSF and plasma NfL concentrations over a 3-month interval in response to mHTT lowering in the CNS of YAC128 mice with either 15 µg or 50 µg HTT ASO initiated at either 2 (Fig. 4) or 12 months of age (Fig. 5). We then assessed biofluid NfL concentrations over a 6-month interval in response to mHTT lowering in the CNS of YAC128 with high dose HTT ASO initiated at 8 months of age (Fig. 6).

Mice: Experiments were performed using YAC128 mice and WT littermate controls. Approximately equal numbers of male and female mice were used for each experiment. Animals were maintained under a 12 hour (h) light : dark cycle in a clean barrier facility and given *ad libitum* access to food and water. Experiments were performed with the approval of the Animal Care Committee at the University of British Columbia (A16-030 and A20-0107).

Saphenous blood collection

Survival blood collection was performed via the saphenous vein where whole blood was drawn using EDTA-coated capillary blood collection tubes (Sarstedt, catalog # 16.444.100) and placed on ice. Whole blood was then centrifuged at 4000 relative centrifugal force (RCF) for 10 minutes (min) at 4^{o}C, plasma was carefully removed, separated into aliquots, flash frozen in liquid N_2 and stored at -80^{o}C until use.

CSF collection

Terminal CSF was collected as previously described (39, 74). Briefly, mice were anesthetized with Avertin (2,2,2-tribromoethanol, Sigma Aldrich, catalog # T48402) and secured in a stereotaxic frame (Stoelting). The ear bars were raised and the nose piece used to position the mice in a manner that would allow for a near 90° tilt of the head to access the cisterna magna. A 1cm^2 section of dorsal neck skin was removed and muscle layers were completely dissected away to expose the cisterna magna, which was then cleaned and dried. A 50 µL Hamilton syringe with a 26 gauge (G) point style 2 needle with a 12^{o} bevel was then lowered carefully into the cisterna magna. CSF was slowly withdrawn at a rate of 10 µL/min using an UltraMicroPump with Micro4 controller (World Precision Instruments). CSF samples were centrifuged, then flash frozen in liquid N_2 and stored at -80^{o}C.

Plasma and CSF NfL analysis

NfL concentrations (pg/mL) were measured in mouse plasma and CSF using the commercially available NF-Light kit (Quanterix, catalog # 103186) on the SIMOA HD-1 analyzer (Quanterix, Lexington, MA).

Plasma samples were diluted 1/40 and CSF samples were diluted 1/100 in NF-Light sample diluent provided with the kit prior to loading into the HD-1 analyzer and then analyzed in duplicate as per the manufacturer's instructions. The intra-assay coefficient of variance (CV) for each sample's duplicate measurement was 4.3%. All sample concentrations were above the lower limit of quantification for the assay (0.174 pg/mL).

Tissue collection and processing

Mice allotted for terminal molecular and biochemical analyses were anesthetized using Avertin and CSF was collected as described above. Brains were then removed and placed on ice for 1 min to increase tissue rigidity, then microdissected into different regions (striatum, cortex, hippocampus, cerebellum). Samples were then flash frozen in liquid N_2 and stored at − 80°C until use.

Mice allotted for histology were perfused transcardially with phosphate-buffered saline (PBS) for 4 min then with 4% paraformaldehyde (PFA) in PBS for 3 min. Brains were removed and post-fixed in 4% PFA for 24 h at 4°C. The following day, brains were cryoprotected in 30% sucrose in PBS with 0.01% sodium azide. Once equilibrated, brains were divided into forebrain and cerebellum, and forebrains were frozen on dry ice, mounted in Tissue-TEK O.C.T. compound (Sakura, catalog # 4583), and cut via cryostat (Leica CM3050S) into a series of 25 µm coronal sections free-floating in PBS with 0.01% sodium azide.

Quantitative polymerase chain reaction (qPCR)

Striatum samples were lysed using MP Biomedicals Lysing Matrix D tubes (Fisher Scientific, catalog # MP116913500) and the FastPrep FP120 Cell Disrupter (Thermo Savant). RNA extraction was performed using the RNeasy Mini Kit (Qiagen, catalog # 74106) according to the manufacturer's protocol. cDNA synthesis was performed using the SuperScript III First-Strand Synthesis System (Invitrogen, catalog # 18080051) according to the manufacturer's protocol using 250 ng or 1000 ng of RNA for striatum and cortex, respectively.

For qPCR, primers against mouse *Nefl* (forward 5' GGG TAT GAA CGA AGC TCT GG-3'; reverse 5'-TCT CAG CTC ATT CTC CAG TTT G 3'), *Gfap* (forward 5' GAA AAC CGC ATC ACC ATT CC 3'; reverse 5' CTT AAT GAC CTC ACC ATC CCG 3') and *Rpl13a* (forward 5'-GGA GGA GAA ACG GAA GGA AAA G-3'; reverse 5'-CCG TAA CCT CAA GAT CTG CTT CTT-3') were synthesized by Integrated DNA Technologies. cDNA was diluted 1:3 for the striatum or 1:5 for the cortex in nuclease-free dH_20. SYBR Green PCR Master Mix (ThermoFisher Scientific, catalog # 4368706) reagents were used according to the manufacturer's protocol and the qPCR was run using the Applied Biosystems 7500 Fast Real-Time PCR System (ThermoFisher Scientific). Relative quantitation of transcript levels was performed using the $2^{-\Delta\Delta CT}$ method.

Intrastriatal (IS) injections

IS QA injections were performed as previously described (39, 74). Briefly, mice were anesthetized with 150 mg/kg ketamine and 10 mg/kg xylazine and secured into a stereotaxic frame. The scalp was shaved, sterilized with betaine and 70% ethanol, and an incision made along the midline. The skull was dried to enhance visibility of sutures and landmarks. A dental drill was used to make a burr hole on the right side of the skull at 0.8 mm anterior and 1.8 mm lateral to bregma. A Hamilton syringe with a 26 G needle loaded with 2 µl of QA at 25 nM in sterile PBS was lowered to a depth of 3.5 mm through the burr hole, and the QA was injected at 0.5 µl/min using a micropump. The needle was left in place for 5 min and then withdrawn slowly. Plasma was collected prior to treatment and at 3- and 7-days post-treatment whereas brains and CSF samples were collected at 3- or 7-days post-treatment.

Histology

For detection of degenerating neurons after QA treatment, sections spanning the injection site were stained using Fluoro-Jade C (Biosensis, catalog #TR-100-FJ) according to the manufacturer's protocol. Sections were mounted using ProLong Gold Antifade mountant with DAPI (Invitrogen, catalog # P36941), and imaged with a 2.5× objective using a Zeiss Axioplan 2 microscope (Carl Zeiss).

For visualization of mHTT inclusions in the brain, sections were co-stained with mouse EM48 (Sigma-Aldrich, catalog # MAB5374) and chicken NeuN (Sigma-Aldrich, catalog # ABN91). Primary antibodies were detected with goat anti-mouse AlexaFluor-488 (1:1000, Invitrogen, catalog #A-11029) and goat anti-chicken AlexaFluor-647 (1:500, Invitrogen, catalog # A-21449) secondary antibodies. Sections were then mounted using ProLong Gold Antifade mountant with DAPI (Thermo Fisher Scientific, catalog # P36931) and imaged with a 40× objective using a Leica TCS SP5 laser scanning confocal microscope.

HTT ASO design

A 5-9-5 chimeric gapmer ASO with a fully phosphorothioate-modified backbone and 5 locked-nucleic acid modifications at each wing designed to target intron 22 of the human *HTT* transcript was synthesized by Qiagen (39). For ASO treatments, molecules were diluted to the indicated concentrations in sterile PBS and administered by ICV injection as described below.

ICV injections

Unilateral ICV injections were performed as previously described (74). Briefly, mice were anesthetized with isoflurane and secured into a stereotaxic frame (Stoelting). The scalp was prepared as described above. A Hamilton syringe with a 26 G needle (Hamilton, Reno, NV) was loaded with 10 µL of PBS or HTT ASO diluted in PBS and was punched through the skull at -1 mm lateral, + 0.3 mm anterior and − 3.0 mm ventral from bregma. The PBS and HTT ASO were delivered as a bolus and the needle was left in place for 2 min after injection prior to being withdrawn slowly.

Quantitative immunoblotting

Tissues were lysed through mechanical dissociation and triturated in lysis buffer (50 mM Tris pH 8.0, 150 mM NaCl, 1% NP40, 40 mM β-glycerophosphate, 10 mM NaF) containing protease inhibitors (1 mM Roche Complete mini EDTA free, 1 nM NaVan, 1 mM PMSF, and 5 μM zVAD). Lysates were incubated on ice and vortexed every 5 min for 20 min. Lysates were centrifuged for 15 min at 18,213 RCF at 4°C and the supernatant was collected. Total protein was quantified using the DC protein assay (Bio-Rad, catalog # 5000113 and 5000114). Samples containing 50 μg total protein were prepared using NuPAGE LDS Sample Buffer (Invitrogen, catalog # NP0007) containing 50 mM dithiothreitol (DTT) and denatured at 70°C for 10 min. Quantitative immunoblotting to resolve HTT alleles was performed as previously described (94).

MesoScale Discovery (MSD) aggregate analysis

Quantification of mHTT aggregates in cortical samples from YAC128 mice was performed at Evotec (Hamburg, Germany) by MSD assay using HTT antibodies MW8 (Developmental Studies Hybridoma Bank, catalog # MW8) and 4C9-sulfo as previously described (95).

Statistical analysis

Statistical analyses were performed using GraphPad Prism version 10 (GraphPad) and R statistical software version 4.3.0 (96). Alpha values of < 0.05 were considered significant for all analyses.

NfL concentrations in CSF and plasma were assessed for normality, and were found to be non-normally distributed. Natural log transformation was found to produce a normal distribution, as reported previously in human HD CSF (41–43). Transformed values were used for all analyses, with the exception of **Fig. S1**, where untransformed NfL concentrations are presented to show the trajectories of CSF and plasma NfL over the natural history of disease in YAC128 and WT littermate control mice.

Comparisons between genotype and/or treatment groups were performed using either a two-tailed Student's t-test (2 groups) or ANOVA (more than 2 groups). Comparisons of longitudinal NfL data involving repeated measures of samples from the same animal were performed by mixed-effect ANOVA. Post hoc analyses for ANOVA tests were performed using the Tukey test (one-way or two-way ANOVA) or the Sidak test (two-way ANOVA) to correct for multiple comparisons.

Longitudinal plasma NfL concentrations in response to mHTT lowering were compared over time by treatment group using linear mixed effects models with a random intercept for each animal. To allow for possible nonlinearity over time, we fit time with a 3 degree of freedom natural spline. To allow for differences in shapes in each treatment group, we included an interaction term between these splines and treatment. Models were adjusted for baseline NfL concentrations in Figs. 4, 5 and 6. Results are summarized graphically as fitted values over time (by treatment group) where solid lines denote the mean and shaded bands denote 95% confidence intervals (95% CI) for each treatment condition, as well as estimated mean differences (MD) over time between treatment groups in Tables 1, 2 and 3. The latter were calculated at the average baseline value, and were computed at each time point data where

available. We also presented smoothed curves over time including baseline values in **Supplementary Figs. 4, 7 and 10**. Models were fit using the lmer function in the lme4 package in R (97).

Table 1

Longitudinal plasma NfL contrasts following short duration mHTT lowering in the brain of YAC128 mice initiated at 2 months of age. MD and 95% CI of plasma NfL concentrations between PBS and HTT ASO treatment groups over a 3-month treatment interval.

Contrast	Treatment interval (months)	MD, 95% CI (log pg/mL)	*P*-value
15 µg HTT ASO - PBS	0.5	0.11, -0.16 to 0.38	0.430
	1	0.03, -0.21 to 0.26	0.830
	1.5	-0.01, -0.21 to 0.20	0.959
	2	0, -0.25 to 0.26	0.982
	3	0.05, -0.22 to 0.33	0.696
50 µg HTT ASO - PBS	0.5	0.15, -0.16 to 0.47	0.338
	1	0.24, -0.04 to 0.52	0.098
	1.5	0.21, -0.04 to 0.46	0.093
	2	0.14, -0.15 to 0.44	0.341
	3	0.16, -0.2 to 0.52	0.377
50 µg HTT ASO − 15 µg HTT ASO	0.5	0.04, -0.29 to 0.38	0.796
	1	0.21, -0.09 to 0.52	0.166
	1.5	0.22, -0.05 to 0.48	0.106
	2	0.14, -0.18 to 0.45	0.384
	3	0.11, -0.27 to 0.49	0.578

Table 2

Longitudinal plasma NfL contrasts following short duration mHTT lowering in the brain of YAC128 mice initiated at 12 months of age. MD and 95% CI of plasma NfL concentrations between PBS and HTT ASO treatment groups over a 3-month treatment interval.

Contrast	Treatment interval (months)	MD, 95% CI (log pg/mL)	*P*-value
15 µg HTT ASO - PBS	0.5	-0.03, -0.2 to 0.14	0.718
	1	0.05, -0.10 to 0.20	0.533
	1.5	0.04, -0.10 to 0.17	0.597
	2	-0.03, -0.19 to 0.14	0.755
	3	-0.11, -0.28 to 0.06	0.185
50 µg HTT ASO - PBS	0.5	0.13, -0.06 to 0.32	0.182
	1	0.14, -0.03 to 0.32	0.101
	1.5	0.12, -0.03 to 0.27	0.122
	2	0.04, -0.15 to 0.22	0.700
	3	-0.31, -0.51 to -0.12	**0.002**
50 µg HTT ASO − 15 µg HTT ASO	0.5	0.16, -0.03 to 0.35	0.096
	1	0.10, -0.07 to 0.27	0.264
	1.5	0.08, -0.07 to 0.24	0.267
	2	0.06, -0.12 to 0.24	0.506
	3	-0.20, -0.39 to -0.01	**0.042**

Table 3

Longitudinal plasma NfL contrasts following long duration mHTT lowering in the brain of YAC128 mice initiated at 8 months of age. MD and 95% CI of plasma NfL concentrations between PBS and HTT ASO treatment groups over a 6-month treatment interval.

Contrast	Treatment interval (months)	MD, 95% CI (log pg/mL)	*P*-value
50 µg HTT ASO - PBS	1	-0.06, -0.22 to 0.11	0.497
	2	-0.09, -0.22 to 0.04	0.182
	3	-0.11, -0.25 to 0.03	0.110
	4	-0.11, -0.25 to 0.02	0.104
	5	-0.10, -0.23 to 0.04	0.148
	6	-0.07, -0.24 to 0.10	0.403

Receiver operating characteristic (ROC) curve analysis was used to compare the discriminatory performance of CSF and plasma NfL for distinguishing between genotypes. Simple linear regression was used to evaluate the relationship of longitudinal plasma NfL in YAC128 and WT mice over time, and to assess the relationship of HTT ASO dose on CSF NfL concentrations. Correlation analyses were performed using Pearson's correlation, where coefficient values (Pearson's r) from ± 0.50 to ± 1 were considered strong correlations, ± 0.30 to ± 0.49 were considered moderate correlations and ± 0.10 to ± 0.29 were considered weak correlations.

All bar plots are presented as either scatter dot bar plots or box plots to demonstrate data complexity and variability. Scatter dot bar plots show means from multiple animals ± standard error of the mean. Box and whisker plots show distribution and skewness of data, where boxes represent 25 to 75 percentiles, whiskers represent 5 to 95 percentiles, horizontal lines represent median values and the crosses represent the mean values. Exact *P* values and 95% CI are presented in the text.

Results

Plasma and CSF NfL are elevated over the natural history of disease in YAC128 mice

The natural history of NfL in biofluids was characterized in the YAC128 mouse model of HD. Cross-sectional CSF and plasma were collected from YAC128 and WT littermate control mice at 2, 6, 9, 12 and 15 months of age for measurement of NfL concentrations (Fig. 1A). In a replication cohort, longitudinal plasma samples were collected at monthly intervals from 6–12 months of age for measurement of NfL concentrations (Fig. 1A).

Plasma NfL concentrations in both WT and YAC128 mice increased significantly with age from 2 to 15 months, and NfL concentrations were significantly elevated in YAC128 compared to WT plasma at 9 and 12 months of age (**Supplementary Fig. 1A**, untransformed NfL concentrations; Fig. 1B, natural log transformed NfL concentrations. Two-way ANOVA: genotype $P < 0.0001$, age $P < 0.0001$, interaction $P = 0.008$. 9 months: MD = 0.90 pg/mL, 95% CI = 0.39 to 1.41, ****$P < 0.0001$; 12 months: MD = 0.57 pg/mL, 95% CI = 0.25 to 0.89, ****$P < 0.0001$). Moreover, CSF NfL also increased in both genotypes with age, with NfL concentrations being significantly increased in CSF from YAC128 compared to WT mice from 9 months of age (**Supplementary Fig. 1B**, untransformed NfL concentrations; Fig. 1C, natural log transformed NfL concentrations. Two-way ANOVA: genotype $P < 0.0001$, age $P < 0.0001$, interaction $P < 0.0001$. 9 months: MD = 2.27 pg/mL, 95% CI = 1.61 to 2.93, ****$P < 0.0001$; 12 months: MD = 1.71 pg/mL, 95% CI = 1.18 to 2.23, ****$P < 0.0001$; 15 months: MD = 1.24 pg/mL, 95% CI = 0.84 to 1.64, ****$P < 0.0001$). Consistent with previous reports in HD mutation carriers (41, 43), NfL concentrations in CSF were orders of magnitude higher compared to those in plasma at any given age.

Longitudinal plasma NfL concentrations in both WT and YAC128 mice increased significantly with age (**Supplementary Fig. 1C**, untransformed NfL concentrations; Fig. 1D, natural log transformed NfL

concentrations. Linear regression: WT: Y = 0.1205X + 3.254, R^2 = 0.90, *P* = 0.001. YAC128: Y = 0.2341X + 2.735, R^2 = 0.99, *P* < 0.0001) with YAC128 plasma NfL increasing at a significantly greater rate from 6 to 12 months of age (Fig. 1D. Comparison of slopes: ****P* = 0.0005). A significant interaction of genotype and age on plasma NfL was observed, with NfL concentrations being significantly elevated in YAC128 mice from 9 months of age (Fig. 1D. Mixed-effect analysis: genotype *P* < 0.0001, age *P* < 0.0001, genotype x age *P* < 0.0001. 9 months: MD = 0.71 pg/mL, 95% CI = 0.41 to 1.01, *****P* < 0.0001; 10 months: MD = 0.60 pg/mL, 95% CI = 0.25 to 0.95, ****P* = 0.0002; 11 months: MD = 0.82 pg/mL, 95% CI = 0.50 to 1.14, *****P* < 0.0001; 12 months: MD = 0.68 pg/mL, 95% CI = 0.16 to 1.19, ***P* = 0.005).

A strong positive correlation between NfL concentrations was observed in paired plasma and CSF samples from the same animal in both genotypes at 12 months of age (Fig. 1E. r = 0.63, 95% CI = 0.28 to 0.83, *P* = 0.002). ROC curve analysis was performed to compare the sensitivity and specificity of plasma and CSF NfL for stratifying YAC128 from WT mice at 12 months of age (Fig. 1F). Both biofluids showed strong discrimination between genotypes, with CSF NfL showing superior stratification at this age (Fig. 1F. CSF NfL AUC = 0.99, 95% CI = 0.97 to 1, *P* = 0.0001. Plasma NfL: AUC = 0.81, 95% CI = 0.67 to 0.94, *P* = 0.0003).

Acute neurodegeneration in the striatum of YAC128 mice leads to increased plasma and CSF NfL concentrations

We next assessed the dynamics of biofluid NfL changes in response to acute neurodegeneration in the brain. QA, a neurotoxin known to induce excitotoxicity (98), was administered unilaterally into the striatum of YAC128 mice. NfL concentrations were measured in longitudinal plasma and cross-sectional CSF samples at 3- and 7-days post-treatment (Fig. 2A). Brains were also collected to measure *Nefl* and *Gfap* transcript levels in the injected (ipsilateral) striatal hemisphere (Fig. 2A).

The presence of a striatal lesion following QA administration was confirmed by IHC using the Fluoro-Jade C dye, which stains degenerating neurons (Fig. 2B). Plasma NfL was significantly elevated at 7 days but not 3 days in animals injected with QA compared to PBS (Fig. 2C. Two-way ANOVA: treatment *P* = 0.005, interval *P* < 0.0001, interaction *P* = 0.093. 3 days: MD = 0.28 pg/mL, 95% CI = -0.80 to 1.36, *P* = 0.882; 7 days: MD = 1.43, 95% CI = 0.35 to 2.51, ***P* = 0.007). Notably, administration of QA resulted in a ~ 149% increase of plasma NfL from baseline at 3 days, and > 1000% increase from baseline at the 7-day interval (Fig. 2D. Two-way ANOVA: treatment *P* = 0.037, interval *P* = 0.024, interaction *P* = 0.093. QA compared to PBS at 3 days: MD = 124.9%, 95% CI = -725.10 to 974.90, *P* = 0.915; 7 days: MD = 975.5%, 95% CI = 125.5 to 1826, **P* = 0.026).

CSF NfL concentrations in animals injected with both PBS and QA were higher at the 3 compared to 7-day interval, with NfL levels being significantly increased at both timepoints in animals that received QA (Fig. 2E. Two-way ANOVA: treatment *P* = 0.0003, interval *P* < 0.0001, interaction *P* = 0.176. 3 days: MD = 1.46 pg/mL, 95% CI = 0.70 to 2.21, ***P* = 0.001; 7 days: MD = 0.85 pg/mL, 95% CI = 0.04 to 1.66, **P* = 0.040). A moderate negative correlation of NfL concentrations was observed between paired CSF and

plasma samples with PBS at both timepoints (Fig. 2F. PBS at 3 and 7 days: r = -0.37, 95% CI = -0.91 to 0.63, $P = 0.469$), whereas there was a strong negative correlation in animals injected with QA (Fig. 2F. QA at 3 and 7days: r = -0.87, 95% CI = -0.98 to -0.35, $P = 0.011$).

Nefl transcript levels in the ipsilateral striatum were significantly decreased in QA compared to PBS injected animals at both 3- and 7-days post-injection (Fig. 2G. Two-way ANOVA: treatment $P < 0.0001$, interval $P = 0.403$, interaction $P = 0.394$. 3 days: MD = -0.58, 95% CI = -0.79 to -0.37, $^{****}P < 0.0001$; 7 days: MD = -0.48, 95% CI = -0.69 to -0.27, $^{***}P = 0.0003$). In contrast, *Gfap* expression was significantly upregulated following QA treatment at both 3- and 7- days post-injection (Fig. 2H. Two-way ANOVA: treatment $P < 0.0001$, interval $P < 0.0001$, interaction $P = 0.0002$. 3 days: MD = 10.05, 95% CI = 7.69 to 12.42, $^{****}P < 0.0001$; 7 days: MD = 2.77, 95% CI = 0.40 to 5.14, $^{*}P = 0.024$).

Sustained, dose-dependent lowering of mHTT in the brain of YAC128 mice with a HTT ASO

We performed a time-course experiment to characterize the magnitude and duration of mHTT lowering in the brain in YAC128 mice following ICV administration with two doses of HTT ASO. Dose selection was informed by previous studies using the same HTT ASO (39, 99) with the goal of achieving either 40–50% or 70–85% mHTT reduction in the brain at a 1-month treatment interval with a low or high dose HTT ASO treatment, respectively. We therefore selected 15 µg HTT ASO and 50 µg HTT ASO for all subsequent experiments.

Two-month-old YAC128 mice received a single unilateral ICV injection with either PBS, 15 or 50 µg HTT ASO, and mHTT levels were quantified (94) in different brain regions (cortex, striatum, hippocampus and cerebellum) at 0.5-, 1-, 2- and 3-month post-treatment intervals (Fig. 3A). The HTT ASO used in this study targets the human mutant *HTT* transgene in YAC128 mice without altering levels of mouse Htt (99). Therefore, for all subsequent experiments, we report levels of mHTT protein in the brain as a measure of target engagement.

We observed a significant interaction between treatment condition and interval in all brain regions, with both doses of HTT ASO resulting in a significant a reduction of mHTT compared to PBS in the cortex (Fig. 3B, C. Two-way ANOVA: treatment $P < 0.0001$, timepoint $P < 0.0001$, interaction $P = 0.0319$. HTT ASO compared to PBS: $^{****}P < 0.0001$), striatum (Fig. 3B, D. Two-way ANOVA: treatment $P < 0.0001$, timepoint $P < 0.0001$, interaction $P < 0.0001$. HTT ASO compared to PBS: $^{*}P = 0.018$, $^{****}P < 0.0001$), hippocampus (Fig. 3B, E. Two-way ANOVA: treatment $P < 0.0001$, timepoint $P < 0.0001$, interaction $P < 0.0001$. HTT ASO compared to PBS: $^{***}P = 0.0005$, $^{****}P < 0.0001$) and cerebellum (Fig. 3B, F. Two-way ANOVA: treatment $P < 0.0001$, timepoint $P = 0.0006$, interaction $P < 0.0001$. HTT ASO compared to PBS: $^{***}P = 0.0001$, $^{****}P < 0.0001$).

As expected, we observed a greater magnitude of mHTT lowering with 50 µg compared to 15 µg HTT ASO in each brain region at all time points assessed (Fig. 3B-F. Cortex: $^{\#\#\#\#}P < 0.0001$; striatum: $^{\#}P = 0.046$, $^{\#\#\#}P = 0.0001$, $^{\#\#\#\#}P < 0.0001$; hippocampus: $^{\#\#\#}P = 0.0007$, $^{\#\#\#\#}P < 0.0001$; cerebellum: $^{\#}P =$

0.017, $^{\#\#\#\#}P < 0.0001$). For both doses of HTT ASO, the highest magnitude of mHTT lowering in all brain regions was observed at approximately 1-month post-treatment (Fig. 3B-F. 15 µg HTT ASO in cortex: MD = -49.51%, 95% CI = -66.88 to -32.14; striatum: MD = -49.29%, 95% CI = -65.85 to -32.72; hippocampus: MD = -64.03%, 95% CI = -78.19 to -49.87; cerebellum: MD = -51.85%, 95% CI = -64.78 to -38.91. 50 µg HTT ASO in cortex: MD = -87.11%, 95% CI = -103.6 to -70.64; striatum: MD = -83.49%, 95% CI = -99.21 to -67.78; hippocampus: MD = -92.51%, 95% CI = -105.90 to -79.08; cerebellum: MD = -66.38%, 95% CI = -78.65 to -54.11).

At the 3-month interval, mHTT levels in 15 µg HTT ASO-treated animals were trending back towards baseline (Fig. 3B-F. Cortex: MD = -16.00%, 95% CI = -32.48 to 0.47; striatum: MD = -18.38%, 95% CI = -34.10 to 2.67; hippocampus: MD = -22.64%, 95% CI = -36.07 to -9.21; cerebellum: MD = -21.91%, 95% CI = -34.18 to -9.64), whereas more sustained mHTT reduction was observed with 50µg HTT ASO in all brain regions up to this timepoint (Fig. 3B-F. Cortex: MD = -55.69%, 95% CI = -72.17 to -39.21; striatum: MD = -33.40%, 95% CI = -49.11 to -17.68; hippocampus: MD = -65.97%, 95% CI = -79.40 to -52.54; cerebellum: MD = -61.05%, 95% CI = -73.32 to -48.78).

We extended our time-course with 50 µg HTT ASO to include measurement of mHTT at 4-, 5- and 6-month post-treatment intervals (**Supplementary Fig. 2A**). Levels of mHTT in the cortex were not significantly decreased with 50 µg HTT ASO from the 4-month treatment interval (**Supplementary Fig. 2B.** Two-way ANOVA: treatment $P = 0.011$, timepoint $P = 0.298$, interaction $P = 0.510$). In contrast, mHTT was significantly reduced in the striatum (**Supplementary Fig. 2C.** Two-way ANOVA: treatment $P = 0.005$, timepoint $P = 0.078$, interaction $P = 0.746$. $^{*}P = 0.034$) and the hippocampus (**Supplementary Fig. 2D.** Two-way ANOVA: treatment $P = 0.001$, timepoint $P = 0.857$, interaction $P = 0.008$. $^{****}P < 0.0001$) at the 4-month interval with 50 µg HTT ASO and returned to near baseline levels at the 5-month interval. In the cerebellum, mHTT was significantly decreased after 4 and 5 months with 50 µg HTT ASO, and returned to near baseline levels at the 6-month treatment interval (**Supplementary Fig. 2E.** Two-way ANOVA treatment $P < 0.0001$, timepoint $P = 0.022$ and interaction $P = 0.0003$. $^{****}P < 0.0001$). For subsequent studies, short and long duration mHTT lowering is used to describe 3- and 6-month treatment paradigms, respectively.

Lowering mHTT in the brain of YAC128 mice prior to motor deficits and regional forebrain atrophy leads to a reduction of CSF NfL concentrations

We evaluated longitudinal plasma NfL and cross-sectional CSF NfL over a 3-month interval in response to low or high dose HTT ASO treatment in the brain of YAC128 mice initiated at 2 months of age (Fig. 4A). Brains were collected at 3 months post-treatment to measure levels of full-length, soluble mHTT protein and *Gfap* mRNA expression in the cortex, striatum, hippocampus and cerebellum (Fig. 4A).

A significant interaction between treatment condition and brain region was observed on mHTT levels at the 3-month treatment interval (Fig. 4B, C. Two-way ANOVA: treatment $P < 0.0001$, brain region $P < 0.0001$, interaction $P = 0.0001$). Full-length, soluble mHTT was significantly reduced in the cortex,

striatum, hippocampus and cerebellum following treatment with 15 µg HTT ASO (Fig. 4B, C. 15 µg HTT ASO compared to PBS in cortex: MD = -13.28%, 95% CI = -23.25 to -3.31, $^{**}P = 0.006$; striatum: MD = -12.15%, 95% CI = -22.12 to -2.17, $^{*}P = 0.013$; hippocampus: MD = -22.37%, 95% CI = -32.35 to -12.40, $^{****}P < 0.0001$; cerebellum: MD = -25.12%, 95% CI = -35.09 to -15.15, $^{****}P < 0.0001$) and 50 µg HTT ASO at the 3-month post-treatment interval (Fig. 4B, C. 50 µg HTT ASO compared to PBS in cortex: MD = -60.70%, 95% CI = -71.88 to -49.51, $^{****}P < 0.0001$; striatum: MD = -34.90%, 95% CI = -46.09 to -23.72, $^{****}P < 0.0001$; hippocampus: MD = -64.59%, 95% CI = -75.77 to -53.40, $^{****}P < 0.0001$; cerebellum: MD = -61.24%, 95% CI = -72.43 to -50.05, $^{****}P < 0.0001$. 50 µg HTT ASO compared to 15 µg HTT ASO in cortex: MD = -47.42%, 95% CI = -59.30 to -35.54, $^{\#\#\#\#}P < 0.0001$; striatum: MD = -22.76%, 95% CI = -34.64 to -10.88, $^{\#\#\#\#}P < 0.0001$; hippocampus: MD = -42.21%, 95% CI = -54.10 to -30.33, $^{\#\#\#\#}P < 0.0001$; cerebellum: MD = -36.12%, 95% CI = -48.00 to -24.24, $^{\#\#\#\#}P < 0.0001$). *Gfap* expression was not altered following treatment with 50 µg HTT ASO compared to PBS in any brain region assessed (**Supplementary Fig. 3**. Two-way ANOVA: treatment $P = 0.558$, brain region $P = 0.558$, interaction $P = 0.060$).

Longitudinal concentrations of plasma NfL were not significantly changed in response to treatment with either 15 or 50 µg HTT ASO compared to PBS over a 3-month interval (**Supplementary Fig. 4**, model unadjusted for baseline NfL; Fig. 4D, model adjusted for baseline NfL. Linear mixed-effects model: treatment $P = 0.151$, treatment x time interaction $P = 0.983$). Treatment with 15 µg HTT ASO showed little effect on plasma NfL concentrations at any timepoint over the 3-month interval (Table 1). YAC128 mice treated with 50 µg HTT ASO showed a trend towards increased plasma NfL compared to PBS at each timepoint over the 3-month interval, which was highest at 1-month post-treatment (Table 1. MD = 0.24 pg/mL, 95% CI = -0.04 to 0.52, $P = 0.098$). Plasma NfL concentrations were not significantly different between the 15 and 50 µg HTT ASO treatments at any timepoint (Table 1). The mean percent change from baseline of plasma NfL at the 3-month post-treatment interval was an increase of 91.27%, 54.25% and 37.34% with PBS, 15 µg HTT ASO and 50 µg HTT ASO, respectively (Fig. 4E. Mixed-effects model: treatment $P = 0.190$, time $P = 0.396$, treatment x time $P = 0.998$).

A significant dose-dependent reduction of cross-sectional CSF NfL was measured in response to HTT ASO treatment (Fig. 4F. Linear regression: $Y = -0.0068X + 6.520$, $R^2 = 0.12$, $P = 0.016$), where CSF NfL concentrations were significantly decreased with 50 µg HTT ASO compared to PBS at the 3-month treatment interval (One-way ANOVA: P = 0.032. 15 µg HTT ASO compared to PBS: MD = -0.22 pg/mL, 95% CI = -0.50 to 0.06, $P = 0.147$; 50 µg HTT ASO compared to PBS: MD = -0.34 pg/mL, 95% CI = -0.67 to -0.01, $P = 0.044$; 50 µg HTT ASO compared to 15 µg HTT ASO: -0.12 pg/mL, 95% CI = -0.47 to 0.24, $P = 0.701$).

A moderate positive correlation was measured between NfL concentrations from matched plasma and CSF samples at the 3-month post-treatment interval (Fig. 4G. r = 0.43, 95% CI = 0.16 to 0.64, $P = 0.003$). Relative mHTT levels in the brain following treatment with PBS, 15 µg or 50 µg HTT ASO showed a weak negative correlation with plasma NfL (Fig. 4H. r = -0.06, 95% CI = -0.37 to 0.25, $P = 0.702$) and a significant positive correlation with CSF NfL (Fig. 4I. r = 0.35, 95% CI = 0.02 to 0.61, $P = 0.041$).

Plasma and CSF NfL concentrations are stabilized in response to mHTT lowering in the brain initiated after onset of striatal neuron loss in YAC128 mice

We next evaluated longitudinal plasma NfL and cross-sectional CSF NfL over a 3-month interval in response to low and high dose HTT ASO treatment in the brain of YAC128 mice initiated at 12 months of age (Fig. 5A). Brains were collected at 3 months post-treatment to measure levels of full-length, soluble mHTT protein in multiple brain regions as well as aggregated mHTT load in the cortex (Fig. 5A).

We measured a dose-dependent reduction of full-length, soluble mHTT in the cortex, striatum, hippocampus and cerebellum of YAC128 mice at the 3-month interval following HTT ASO treatment (Fig. 5B, C. Two-way ANOVA: treatment $P < 0.0001$, brain region $P < 0.0001$, interaction $P = 0.0009$. 15 µg HTT ASO compared to PBS in cortex: MD = -21.70%, 95% CI = -32.60 to -11.13, ****$P < 0.0001$; striatum: MD = -15.31%, 95% CI = -25.87 to -4.74, **$P = 0.002$; hippocampus: MD = -32.74%, 95% CI = -43.31 to -22.18, ****$P < 0.0001$; cerebellum: MD = -38.89%, 95% CI = -49.46 to -28.33, ****$P < 0.0001$. 50 µg HTT ASO compared to PBS in cortex: MD = -68.06%, 95% CI = -78.05 to -58.06, ****$P < 0.0001$; striatum: MD = -57.05%, 95% CI = -67.05 to -47.05, ****$P < 0.0001$; hippocampus: MD = -76.27%, 95% CI = -86.27 to -66.28, ****$P < 0.0001$; cerebellum: MD = -67.11%, 95% CI = -77.10 to -57.11, ****$P < 0.0001$. 50 µg HTT ASO compared to 15 µg HTT ASO in cortex: MD = 46.36%, 95% CI = -57.71 to -35.01, $^{####}P < 0.0001$; striatum: MD = -41.74%, 95% CI = -53.10 to 30.39, $^{####}P < 0.0001$; hippocampus: MD = -43.53%, 95% CI = -54.88 to -32.18, $^{####}P < 0.0001$; cerebellum: MD = -28.21%, 95% CI = -39.56 to -16.86, $^{####}P < 0.0001$).

Compared to short duration mHTT lowering initiated at 2 months of age (Fig. 4C), treatment with both 15 µg HTT ASO and 50 µg HTT ASO resulted in a significantly greater magnitude of mHTT lowering in the brain at the 3-month post-treatment interval when initiated at 12 months of age (**Supplementary Fig. 5**. Two-way ANOVA: treatment $P < 0.0001$, age $P < 0.0001$, interaction $P = 0.007$. 15 µg HTT ASO: MD = -8.93%, 95% CI = -16.92 to -0.95, *$P = 0.023$. 50 µg HTT ASO: MD = -13.43%, 95% CI = -21.80 to -5.06, ***$P = 0.0006$).

YAC128 mice develop distinct mHTT inclusion bodies in the brain from 12 months of age (87, 91), a hallmark neuropathological feature of HD (100). We observed a progressive, age-dependent increase of mHTT inclusions (**Supplementary Fig. 6A**. One-way ANOVA: $P = 0.011$. 12 compared to 8 months: MD = 29.69 fmol/mg, 95% CI = -49.70 to 109.10, $P = 0.609$. 18 compared to 8 months: MD = 94.69 fmol/mg, 95% CI = 19.95 to 169.40, *$P = 0.013$. 18 compared to 12 months: MD = 65.01 fmol/mg, 95% CI = -5.80 to 135.80, $P = 0.075$) and a corresponding reduction of full-length, soluble mHTT in the cortex of YAC128 mice from 8 to 18 months of age (**Supplementary Fig. 6B.** One-way ANOVA: $P = 0.038$. 12 compared to 8 months: MD = -0.08, 95% CI = -0.32 to 0.17, $P = 0.720$. 18 compared to 8 months: MD = -0.24, 95% CI = -0.46 to -0.02, *$P = 0.034$. 18 compared to 12 months: MD = -0.16, 95% CI = -0.40 to 0.08, $P = 0.225$).

A significant dose-dependent reduction of mHTT inclusion load was measured in the cortex of HTT ASO-treated YAC128 mice at 3 months post-treatment (**Supplementary Fig. 6C**. One-way ANOVA: $P = 0.0002$. 15 µg HTT ASO compared to PBS: MD = -29.62 fmol/mg, 95% CI = -50.11 to -9.140, **$P = 0.004$. 50 µg

HTT ASO compared to PBS: MD = -48.28 fmol/mg, 95% CI = -76.13 to -20.44, ***P = 0.0006) which was accompanied by a qualitative reduction of EM48 + neuronal mHTT inclusions in the striatum with 50 µg HTT ASO by IHC (**Supplementary Fig. 6D**). A strong positive correlation was observed between relative soluble mHTT and aggregated mHTT levels from matched cortical samples following short duration mHTT lowering initiated at 12 months of age (**Supplementary Fig. 6E**. r = 0.81, 95% CI = 0.61 to 0.91, P< 0.0001).

A significant treatment by time interaction on plasma NfL concentrations was observed over a 3-month interval in response to HTT ASO treatment initiated at 12 months of age (**Supplementary Fig. 7**, model unadjusted for baseline NfL; Fig. 5D, model adjusted for baseline NfL. Linear mixed-effects model: treatment P = 0.790, treatment x time interaction P = 0.001). Plasma NfL concentrations were not significantly changed at any timepoint in response to treatment with 15 µg HTT ASO compared to PBS over the treatment interval (Table 2). In contrast, a trend towards increased plasma NfL was measured in response to 50 µg HTT ASO treatment up to the 2-month treatment interval, followed by a significant reduction at the 3-month timepoint compared to PBS (MD = -0.31 pg/mL, 95% CI = -0.51 to -0.12, P = 0.002) and 15 µg HTT ASO (MD = -0.20 pg/mL, 95% CI = -0.39 to -0.01, P = 0.042). The mean percent change from baseline of plasma NfL was an increase of 36.20% with PBS and 11.81% with 15 µg HTT ASO, and a decrease of 16.18% with 50 µg HTT ASO at the 3-month post-treatment interval (Fig. 5E. Mixed-effects model: treatment P = 0.057, time P = 0.039, treatment x time P = 0.015. 50 µg HTT ASO compared to PBS: MD = -52.38%, 95% CI = -91.14 to -13.62, **P = 0.003; 15 µg HTT ASO compared to PBS: MD = -24.39%, 95% CI = -53.72 to 4.95, P = 0.181; 50 µg HTT ASO compared to 15 µg HTT ASO: MD = -27.99, 95% CI = -64.69 to 8.70, P = 0.257).

A significant dose-dependent reduction of cross-sectional CSF NfL was measured in response to HTT ASO treatment (Linear regression: Y = -0.0057X + 9.117, R^2 = 0.16, P = 0.011), where CSF NfL concentrations were significantly decreased with 50 µg HTT ASO compared to PBS at the 3-month treatment interval (One-way ANOVA: P = 0.025. 15 µg HTT ASO compared to PBS: MD = -0.19 pg/mL, 95% CI = -0.47 to 0.08, P = 0.215; 50 µg HTT ASO compared to PBS: MD = -0.29 pg/mL, 95% CI = -0.55 to -0.03, P = 0.024; 50 µg HTT ASO compared to 15 µg HTT ASO: -0.10 pg/mL, 95% CI = -0.40 to 0.20, P = 0.696).

A weak positive correlation was observed between NfL concentrations from matched plasma and CSF samples at the 3-month post-treatment interval (Fig. 5G. r = 0.25, 95% CI = -0.07 to 0.53, P = 0.132). Relative mHTT levels in the brain showed a significant positive correlation with both plasma NfL (Fig. 5H. r = 0.35, 95% CI = 0.04 to 0.60, P = 0.031) and CSF NfL (Fig. 5I. r = 0.42, 95% CI = 0.12 to 0.65, P = 0.009) following treatment with PBS, 15 µg or 50 µg HTT ASO at this timepoint.

Sustained reduction of mHTT in the brain of YAC128 mice initiated prior to overt striatal neuron loss stabilizes increase of plasma and CSF NfL

We next evaluated longitudinal plasma NfL and cross-sectional CSF NfL over a 6-month interval in response to high dose HTT ASO treatment in the brain of YAC128 mice initiated at 8 months of age.

(Fig. 6A). Brains were collected at 3 months post-treatment to assess target engagement of full-length, soluble mHTT in multiple brain regions and aggregated mHTT in the cortex (Fig. 6A).

Levels of full-length, soluble mHTT were significantly reduced in the cortex, striatum, hippocampus and cerebellum of YAC128 mice with 50 µg HTT ASO at the 6-month treatment interval (Fig. 6B **and C**. Two-way ANOVA: treatment $P < 0.0001$, brain region $P < 0.0001$, interaction $P < 0.0001$. 50 µg HTT ASO compared to PBS in cortex: MD = -22.77%, 95% CI = -32.27 to -13.27, ****$P < 0.0001$; striatum: MD = -15.59%, 95% CI = -25.09 to -6.08, ***$P = 0.0003$; hippocampus: MD = -31.10%, 95% CI = -40.60 to -21.60, ****$P < 0.0001$; cerebellum: MD = -42.03%, 95% CI = -51.53 to -32.53, ****$P < 0.0001$). Compared to long duration mHTT lowering with 50 µg HTT ASO initiated at 2 months of age, the relative magnitude of mHTT lowering with this dose was significantly greater when initiated at 8 months of age (**Supplementary Fig. 8**. Two-way ANOVA: treatment $P < 0.0001$, age $P < 0.0001$, interaction $P < 0.0001$. 8 compared to 2 months: MD = -21.10%, 95% CI = -28.37 to -13.83, ****$P < 0.0001$).

We also measured a significant reduction of aggregated mHTT in the cortex following treatment with 50 µg HTT ASO (**Supplementary Fig. 9A**. MD = -41.71 fmol/mg, 95% CI = -58.67 to -24.75, ****$P < 0.0001$), and a strong positive correlation between relative soluble mHTT (Fig. 6C) and aggregated mHTT levels from paired cortical samples at the 6-month interval (**Supplementary Fig. 9B**. r = 0.71, 95% CI = 0.42 to 0.87, $P = 0.0002$).

A strong trend towards a significant treatment effect on plasma NfL concentrations was observed over a 6-month interval in response to 50 µg HTT ASO treatment initiated at 8 months of age (**Supplementary Fig. 10**, model unadjusted for baseline NfL; Fig. 6D, model adjusted for baseline NfL. Linear mixed-effects model: treatment $P = 0.056$, treatment x time interaction $P = 0.934$). A sustained stabilization of plasma NfL increase was measured with 50 µg HTT ASO compared to PBS over the 6-month treatment interval, showing the greatest effect at 3- and 4-months post-treatment (Table 3. 3 months: MD = -0.11 pg/mL, 95% CI = -0.25 to 0.03, $P = 0.110$; 4 months: MD = -0.11 pg/mL, 95% CI = -0.25 to 0.02, $P = 0.104$). The mean percent change from baseline of plasma NfL at the 3-month post-treatment interval was an increase of 106.25% with PBS compared to 67.50% with 50 µg HTT ASO (Fig. 6E. Mixed-effects model: treatment $P = 0.411$, time $P < 0.0001$, treatment x time $P = 0.565$. MD = -38.74%, 95% CI = -100.40 to 22.91, $P = 0.408$). At the 6-month post-treatment interval, plasma NfL concentrations were increased from baseline by 119.99% with PBS compared to 101.72% with 50 µg HTT ASO (MD = -18.28%, 95% CI = -110.70 to 74.19, $P = 0.993$).

Cross-sectional CSF NfL concentrations were significantly increased with PBS but not with 50 µg HTT ASO at the 6-month treatment interval compared to baseline levels at 8 months of age (Fig. 6F. One-way ANOVA: $P = 0.0007$. PBS compared to baseline: MD = 0.58 pg/mL, 95% CI = 0.24 to 0.92, ***$P = 0.0007$; 50 µg HTT ASO compared to baseline: MD = 0.21 pg/mL, 95% CI = -0.14 to 0.57, $P = 0.307$). Notably, CSF NfL concentrations were significantly decreased with 50 µg HTT ASO compared to PBS at the 6-month treatment interval (MD = -0.36 pg/mL, 95% CI = -0.67 to -0.05, *$P = 0.020$).

A moderate positive correlation was observed between NfL concentrations from matched plasma and CSF samples at the 6 months post-treatment interval (Fig. 6G. r = 0.37, 95% CI = -0.04 to 0.68, *P* = 0.082). Relative mHTT levels in the brain showed a moderate positive correlation with plasma NfL concentrations (Fig. 6H. r = 0.34, 95% CI = -0.09 to 0.66, *P* = 0.117) and a significant positive correlation with CSF NfL (Fig. 6I. r = 0.78, 95% CI = 0.54 to 0.90, *P* < 0.0001) at this interval following treatment with PBS and 50 µg HTT ASO.

Discussion

Therapies aimed at lowering mHTT in the CNS have emerged as promising therapeutic approaches for treating HD. Preclinical studies have shown that lowering mHTT in the brain can prevent regional forebrain atrophy and neurodegeneration in HD rodent models (12–14). These findings have accelerated clinical development and therapeutic trials of various HTT lowering modalities for HD. NfL has been validated in multiple well-powered studies as a sensitive and robust biomarker for monitoring disease severity, progression and prognostic outcome in HD (41–45) and has been included as an exploratory endpoint in clinical trials for HD (15, 20–22). However, little is known of whether NfL in biofluids could be used as a response biomarker to assess efficacy of candidate disease-modifying therapies for HD. To address this gap in knowledge, we investigated the relationship of NfL concentrations in CSF and plasma in response to mHTT lowering in the brain of YAC128 mice. Moreover, the impact of timing and magnitude of mHTT lowering was assessed on NfL concentrations in biofluids from YAC128 mice. We chose the YAC128 model, in part because it permits selective lowering of human mutant HTT without altering expression of the animal's two wild-type alleles, excluding wild-type HTT deficiency as a mechanism for possible NfL alteration.

We characterized the natural history of NfL in plasma and CSF from YAC128 and WT littermate control mice. Concentrations of NfL in CSF were orders of magnitude higher compared to those in plasma at any given age. We observed an age-dependent increase of NfL in plasma and CSF from both genotypes, which is consistent with the reported correlation of NfL in biofluids with age in healthy individuals (101) and HD mutation carriers (43). Notably, plasma and CSF NfL concentrations in YAC128 were significantly elevated compared to WT mice from 9 months of age, which corresponds with the earliest reported loss of striatal neurons in YAC128 mice (87). Moreover, longitudinal plasma NfL in YAC128 mice increased with age at a greater rate compared to WT littermate controls, which is consistent with the reported rise of NfL concentrations in biofluids with HD severity and progression (43). We also observed an apparent slowing of NfL increase in CSF from 12 months and plasma from 15 months in YAC128 mice, consistent with observations that the slope steepness trajectories associated with plasma and CSF NfL concentrations decrease with age in HD mutation carriers (42). Taken together, these data demonstrate that biofluid NfL concentrations in YAC128 mice may accurately model the changes observed in HD patients.

Importantly, a strong positive correlation of NfL concentrations between paired plasma and CSF concentrations was measured at 12 months of age in WT and YAC128 mice. CSF flow and exchange

with the blood compartment plays an important role in the clearance of solutes from the brain interstitial space (102). The association of NfL concentrations between biofluids suggests that both CSF and plasma NfL reflect the same pathophysiological perturbations in the brain of YAC128 mice. We observed that CSF NfL showed superior discrimination of YAC128 and WT control mice at 12 months of age, suggesting that CSF NfL may be a more robust marker of neurodegeneration and therefore a more sensitive for measuring the response to mHTT lowering in the brain of YAC128 mice. However, CSF collection from the cisterna magna of mice is typically a terminal procedure, limiting our study to cross-sectional analyses of CSF NfL concentrations. In contrast, plasma collection via saphenous vein is relatively non-invasive and can be performed repeatedly from the same animal, allowing for monitoring of longitudinal NfL dynamics.

QA, a glutamate agonist, induces excitotoxicity by binding and potentiating NMDA receptors in neurons (103). We evaluated NfL in matched CSF and plasma samples in response to QA-induced acute neurodegeneration in the striatum of YAC128 mice to assess the temporal dynamics of NfL changes in this model. We observed a significant elevation of CSF NfL with QA-administration at both 3- and 7-days post-injection, where the magnitude of CSF NfL was highest at the 3-day interval. In contrast, we measured a significant increase of plasma NfL at 7-days but not 3 days after QA administration, where a strong negative correlation was measured between CSF and plasma NfL. Together these data suggest that NfL is rapidly released from degenerating neurons in the brain to the CSF in response to neurotoxic insult, and more slowly cleared from the CSF to the blood compartment. The delayed increase in plasma NfL following neuronal injury is also consistent with the elevated serum NfL levels in boxers 7–10 days after a bout (69). The sensitive, robust and relatively rapid response of NfL in biofluids to acute neurotoxicity in the brain suggests that NfL could be useful as a safety biomarker in early phase clinical trials to flag candidate drugs that are poorly tolerated and adversely affect neuronal health, as well as help guide appropriate dosing and treatment paradigms. As an example, the transient dose-dependent increase of CSF NfL in response to tominersen treatment in the phase I/II trial (85), which was also subsequently observed with the 120 mg tominersen every 8 weeks dosing regimen in the GENERATION HD1 phase III trial (86), could have been used as an early indicator to suggest that the drug may have neurotoxic properties at higher doses and/or more frequent treatment intervals.

Intrathecal delivery of ASOs into the subarachnoid space of the spinal cord has been used in clinical trials for HD (16–19, 84–86) and other neurodegenerative diseases, such as SMA (104). This route of administration bypasses the blood-brain barrier, but drugs are subject to rapid efflux from the CSF and limited diffusion into the brain parenchyma. ASOs delivered into the CSF result in target RNA suppression in many cell types of the brain, including neurons and glia (105). Preclinical studies in rhesus macaques have demonstrated that intrathecally-delivered ASOs distribute unevenly throughout the brain, resulting in a concentration gradient where ASO levels are highest in brain regions proximal to CSF, and lower in areas more distal from the CSF compartment (12, 13). *Post mortem* analysis of the brain from a participant treated with tominersen suggests that a similar distribution gradient of ASO occurs in human adults (Dr. Blair Leavitt; CHDI HDTC 2023 presentation).

ICV delivery into CSF of the lateral ventricle can be reliably performed in mice and was used in our study as an analogous route to the intrathecal mode of administration used in clinical trials to deliver ASOs to the CNS. We and others have previously shown that ICV infusion of HTT lowering ASOs results in broad distribution and mHTT lowering throughout the CNS in rodent models of HD (13, 99, 106). Consistent with these reports, we found that a single unilateral ICV injection with either 15 or 50 µg HTT ASO initiated at either 2 or 12 months of age in YAC128 mice was well tolerated and resulted in dose-dependent reduction of full-length, soluble mHTT in multiple brain structures (eg. cortex, striatum, hippocampus and cerebellum) following a 3-month treatment interval. Moreover, high-dose HTT ASO treatment initiated at 8 months of age resulted in a sustained reduction of soluble mHTT throughout the brain up to 6 months of post-treatment. Notably, we observed that mHTT reduction throughout the brain was greater with the same dose of HTT ASO when treatment was initiated in older YAC128 mice, when HD-like phenotypes in this model are more severe, suggesting that age at treatment with HTT ASO can impact the magnitude of mHTT lowering in the brain. Dysfunction of the glymphatic system has been reported in HD (107), which we hypothesize may contribute to reduced clearance of ASOs and other solutes (eg. mHTT) from the brain parenchyma at older ages in YAC128 mice. This is further supported by reports showing that glymphatic function is impaired in neurodegenerative disease (reviewed in (108)) and in the aging brain (109, 110). Our findings suggest that disease severity and age may influence the distribution and/or uptake of ASO in the brain, and may have implications for the design of dosing paradigms for HD clinical trials.

Inclusion bodies composed of aggregated mHTT within neurons of the CNS are a hallmark neuropathological feature of HD (100). Widespread mHTT inclusion bodies have been reported in the cortex and striatum of YAC128 mice from as early as 6 months of age (111), where the number and size of mHTT aggregates increase with age (87, 91). Consistent with these findings, we measured an age-dependent increase in mHTT inclusion load in the cortex of YAC128 mice from 8 to 18 months of age, which was coincident with a reduction of full-length, soluble mHTT. These data highlight an age-dependent transition from soluble to aggregated mHTT in this mouse model.

As part of our study, we also investigated the impact of HTT ASO treatment in the CNS on mHTT inclusion load in the brain of YAC128 mice. We found that mHTT lowering initiated in the CNS of YAC128 mice early (at 8 months) and later (at 12 months) during mHTT inclusion formation led to a significant reduction in mHTT inclusion load in the cortex and correlated strongly with levels of soluble mHTT from paired cortical samples. Other groups have previously reported sustained reduction of mHTT aggregate load in YAC128 mice following treatment with virally-encoded RNAi modalities targeting *HTT* (111–113). However, to our knowledge, this is the first report to demonstrate that transient mHTT lowering in CNS using an ASO leads to a reduction of mHTT aggregates in the brain.

YAC128 mice develop progressive striatal and forebrain atrophy starting at 3 months of age (88, 89), overt motor deficits from 4 months of age (90–92), and robust striatal neuron loss (up to 18%) by 12 months of age (87). Based on the extensive phenotypic characterization of this HD mouse model, we designed our study to evaluate the response of NfL in biofluids to mHTT lowering in the brain initiated at

different ages in YAC128 mice to model therapeutic intervention during the premanifest (pre-symptomatic) and manifest (symptomatic) stages of HD.

YAC128 mice at 2 months of age model a pre-symptomatic stage of disease where animals do not display overt behavioural phenotypes, regional brain atrophy or neurodegeneration. Consistent with this finding, we did not measure a significant genotypic difference in plasma or CSF NfL concentrations at this age. HTT ASO treatment initiated at 2 months of age resulted in dose-dependent reduction of soluble mHTT throughout the brain (~ 18% and 54% with 15 and 50 µg HTT ASO, respectively) without any measurable induction of gliosis. Plasma NfL concentrations were not significantly changed in response to mHTT lowering over the 3-month treatment interval. In contrast, a dose-dependent reduction of CSF NfL was measured following HTT ASO treatment, where there was a significant positive correlation between the magnitude of mHTT lowering in the brain and corresponding CSF NfL concentrations. Our data suggests that CSF NfL is a more sensitive response biomarker when intervention is initiated prior to overt brain atrophy and neurodegeneration in YAC128 mice. This may be due to the higher baseline levels of NfL in CSF compared to plasma at the pre-symptomatic stage of disease, thus providing a greater window to detect a decrease of NfL.

YAC128 mice at 12 months of age model an advanced symptomatic stage of HD, where animals display behavioural abnormalities, robust regional forebrain atrophy and striatal neuron loss (87–90, 93). At this age, CSF and plasma NfL concentrations were significantly elevated compared to WT littermate control mice. Treatment of 12-month-old YAC128 mice with 15 or 50 µg HTT ASO resulted in a sustained, dose-dependent reduction of soluble (27% and 67%, respectively) and aggregated mHTT (17% and 28%, respectively) in the brain at the 3-month interval. Notably, we observed an interaction between treatment and time on plasma NfL concentrations, where high dose HTT ASO treatment resulted in a significant reduction of absolute plasma NfL concentrations and mean percent change from baseline compared to PBS treatment by 3 months post-treatment. Moreover, a significant dose-dependent reduction of NfL with HTT ASO treatment was measured in paired cross-sectional CSF samples at the 3-month interval. Importantly, significant positive correlations between relative mHTT levels in the brain and NfL concentrations in both plasma and CSF were observed, demonstrating a relationship between the magnitude of mHTT lowering in the brain and the response of NfL in biofluids. Our data suggest that both plasma and CSF NfL are robust response biomarkers when mHTT lowering in the brain is initiated after marked loss of striatal neuron populations in YAC128 mice. We postulate that the stabilization of NfL concentrations in both biofluids may reflect a slowing of neurodegeneration and cell loss at this advanced stage of disease.

YAC128 mice at 8 months of age model an early/mid symptomatic stage of HD where animals display clear behavioural and neuropathological phenotypes, but striatal cell loss may be absent (87, 89, 90, 93). We have previously demonstrated that ASO-mediated mHTT lowering initiated at 6 months in a humanized mouse model of HD ameliorates forebrain atrophy and prevents striatal neurodegeneration at 12 months of age (13). Concentrations of CSF and plasma NfL showed trends towards an increase in YAC128 compared to WT littermate control mice at 8 months of age. High dose HTT ASO treatment of

YAC128 mice initiated at this age resulted in a potent and sustained reduction of soluble (~ 28%) and aggregated mHTT (~ 23%) in the brain at the 6-month interval. This magnitude of mHTT lowering was accompanied by a stabilization of plasma NfL increase compared to PBS treatment over this treatment interval, where the strongest effect was observed at 3–4 months post-treatment. Moreover, CSF NfL concentrations in animals treated with 50 µg HTT ASO were significantly reduced compared those treated with PBS at 6 months post-treatment interval, and were not significantly increased from concentrations at baseline. Our data demonstrate a measurable stabilization of NfL increases in both plasma and CSF in response to mHTT lowering in the brain of YAC128 mice initiated at an age modeling an early-mid symptomatic stage of HD. We postulate that this stabilization of NfL may reflect improved neuronal health and/or slowing of neurodegeneration over a period when active neurodegeneration is occurring in this model.

A limitation of our study is the inability to validate that the measured changes of NfL in response to mHTT lowering in the CNS are directly related to improvements of HD-like behavioural and neuropathological phenotypes. Additional studies incorporating neuropathological analyses and/or imaging-based measures are needed to investigate the relationship between structural changes in the brain and NfL concentrations in biofluids in response to mHTT lowering in the CNS. These studies are necessary to further inform whether NfL could be useful as a response biomarker for monitoring therapeutic efficacy related to neuronal preservation in HD.

Another potential limitation of our study was the use of a single ICV infusion to deliver HTT ASO rather than repeated or continuous infusion of HTT ASO. Lowering of mHTT in the CNS with ASOs is transient, where the duration of reduction following a single dose typically lasts on the order of months (13, 114). An efficacious treatment aimed at modifying the course of HD will therefore likely necessitate repeated administration of the drug to sustain mHTT lowering over extended periods of time. We observed that mHTT lowering with both 15 and 50 µg HTT ASO resulted in peak reduction at ~ 1 month in all brain regions, with levels of mHTT gradually coming back to baseline in a dose-dependent manner over a 6-month time frame. Additional preclinical studies are needed where HTT ASO is administered repeatedly to more accurately model treatment paradigms in clinical trials for HD in order to better understand the dynamics of NfL in biofluids in response to sustained mHTT in the CNS.

Conclusions

In this study, we show evidence that NfL in biofluids respond to mHTT lowering in the CNS, and that the magnitude of mHTT lowering and timing of intervention in the disease course impacts this response in the CSF and plasma. Our data supports the further investigation of NfL as a response biomarker for assessing the efficacy of disease-modifying therapies for HD.

Abbreviations

ALS: amyotrophic lateral sclerosis

ASO: antisense oligonucleotide

AUC: area under the curve

BL: baseline

CBL: cerebellum

CI: confidence interval

CNS: central nervous system

CSF: cerebrospinal fluid

CTX: cortex

CV: coefficient of variance

HD: Huntington disease

HIP: hippocampus

Htt: mouse huntingtin

ICV: intracerebroventricular

IS: intrastriatal

MD: mean difference

mHTT: mutant huntingtin

MS: multiple sclerosis

MSD: mesoscale discovery

NfL: neurofilament light chain

PBS: phosphate-buffered saline

PFA: paraformaldehyde

QA: quinolinic acid

ROC: receiver operating characteristic

qPCR: quantitative polymerase chain reaction

SIMOA: single molecule array

SMA: spinal muscular atrophy

STR: striatum

WT: wild type

Declarations

Ethics approval and consent to participate

All experiments involving animals were performed with the approval of the Animal Care Committee at the University of British Columbia (A16-030 and A20-0107).

Consent for publication

Not applicable

Availability of data and materials

The datasets used and/or analysed during the current study are available from the corresponding author on reasonable request.

Competing interests

DJH and PM are paid employees of F. Hoffmann-La Roche. BRL is a founder and CEO of Incisive Genetics Inc. MRH is the CEO of Prilenia Therapeutics and serves on the public boards of Ionis Pharmaceuticals, Oxford Biomedica, AbCellera and 89bio.

Funding

Support for N.S.C. and L.M.B. provided by the Huntington's Disease Society of America Berman/Topper HD Career Development Fellowship. Project operational support for E.J.W., B.R.L., and M.R.H. provided by F. Hoffmann-La Roche. Additional operational support for N.S.C. and M.R.H. provided by a Bev Hartig Huntington's Disease Foundation grant. Funding sources were not involved in the design of experiments, collection and measurement of samples, or analysis and interpretation of the data presented herein.

Author contributions

NSC and MRH designed the study; NSC, LMB, FLL, JNB, AEA, YK, CA, LC, AMH performed research; NSC and JNB analysed data; NSC drafted the manuscript; NSC, LMB, FLL, AEA, JNB, AMH, DJH, PM, EJW, BRL and MRH reviewed and edited the manuscript. All authors read and approved the final manuscript.

Acknowledgements

The authors would like to thank Madhurima Benekareddy and Scott Schobel for their discussions and feedback of experimental design; Mark Wang for mouse husbandry; Qingwen Xia for animal genotyping; and Rachel Dumbrell for technical support with NfL measurements in biofluids.

References

1. A novel gene containing a trinucleotide repeat that is expanded and unstable on Huntington's disease chromosomes. The Huntington's Disease Collaborative Research Group. Cell. 1993;72(6):971-83.
2. Caron NS, Dorsey ER, Hayden MR. Therapeutic approaches to Huntington disease: from the bench to the clinic. Nat Rev Drug Discov. 2018;17(10):729-50.
3. Deng YP, Albin RL, Penney JB, Young AB, Anderson KD, Reiner A. Differential loss of striatal projection systems in Huntington's disease: a quantitative immunohistochemical study. J Chem Neuroanat. 2004;27(3):143-64.
4. Reiner A, Albin RL, Anderson KD, D'Amato CJ, Penney JB, Young AB. Differential loss of striatal projection neurons in Huntington disease. Proc Natl Acad Sci U S A. 1988;85(15):5733-7.
5. Glass M, Dragunow M, Faull RL. The pattern of neurodegeneration in Huntington's disease: a comparative study of cannabinoid, dopamine, adenosine and GABA(A) receptor alterations in the human basal ganglia in Huntington's disease. Neuroscience. 2000;97(3):505-19.
6. Cudkowicz M, Kowall NW. Degeneration of pyramidal projection neurons in Huntington's disease cortex. Ann Neurol. 1990;27(2):200-4.
7. Hedreen JC, Peyser CE, Folstein SE, Ross CA. Neuronal loss in layers V and VI of cerebral cortex in Huntington's disease. Neurosci Lett. 1991;133(2):257-61.
8. Heinsen H, Strik M, Bauer M, Luther K, Ulmar G, Gangnus D, et al. Cortical and striatal neurone number in Huntington's disease. Acta Neuropathol. 1994;88(4):320-33.
9. Vonsattel JP, Myers RH, Stevens TJ, Ferrante RJ, Bird ED, Richardson EP, Jr. Neuropathological classification of Huntington's disease. J Neuropathol Exp Neurol. 1985;44(6):559-77.
10. Singh-Bains MK, Tippett LJ, Hogg VM, Synek BJ, Roxburgh RH, Waldvogel HJ, et al. Globus pallidus degeneration and clinicopathological features of Huntington disease. Ann Neurol. 2016;80(2):185-201.
11. Liu CF, Younes L, Tong XJ, Hinkle JT, Wang M, Phatak S, et al. Longitudinal imaging highlights preferential basal ganglia circuit atrophy in Huntington's disease. Brain Commun. 2023;5(5):fcad214.
12. Kordasiewicz HB, Stanek LM, Wancewicz EV, Mazur C, McAlonis MM, Pytel KA, et al. Sustained therapeutic reversal of Huntington's disease by transient repression of huntingtin synthesis. Neuron. 2012;74(6):1031-44.

13. Southwell AL, Kordasiewicz HB, Langbehn D, Skotte NH, Parsons MP, Villanueva EB, et al. Huntingtin suppression restores cognitive function in a mouse model of Huntington's disease. Sci Transl Med. 2018;10(461).
14. Caron NS, Southwell AL, Brouwers CC, Cengio LD, Xie Y, Black HF, et al. Potent and sustained huntingtin lowering via AAV5 encoding miRNA preserves striatal volume and cognitive function in a humanized mouse model of Huntington disease. Nucleic Acids Res. 2020;48(1):36-54.
15. Hoffmann-La Roche "A Study to Evaluate the Efficacy and Safety of Intrathecally Administered RO7234292 (RG6042) in Participants With Manifest Huntington's Disease". NCT03761849, 2019.
16. Wave Life Sciences Ltd. "Safety and Tolerability of WVE-120101 in Patients With Huntington's Disease (PRECISION-HD1)". NCT03225833, 2017.
17. Wave Life Sciences Ltd. "Safety and Tolerability of WVE-120102 in Patients With Huntington's Disease (PRECISION-HD2)". NCT03225846, 2017.
18. Wave Life Sciences Ltd. "Study of WVE-003 in Patients With Huntington's Disease". NCT05032196, 2021.
19. Hoffmann-La Roche "GENERATION HD2. A Study to Evaluate the Safety, Biomarkers, and Efficacy of Tominersen Compared With Placebo in Participants With Prodromal and Early Manifest Huntington's Disease". NCT05686551, 2023.
20. Ionis Pharmaceuticals, Inc. "Safety, Tolerability, Pharmacokinetics, and Pharmacodynamics of ISIS 443139 in Participants With Early Manifest Huntington's Disease". NCT02519036, 2015.
21. UniQure Biopharma B.V. "Safety and Proof-of-Concept (POC) Study With AMT-130 in Adults With Early Manifest Huntington Disease". NCT04120493, 2019.
22. UniQure Biopharma B.V. "Safety and Efficacy of AMT-130 in European Adults With Early Manifest Huntington Disease". NCT05243017, 2022.
23. PTC Therapeutics "A Study to Evaluate the Safety and Efficacy of PTC518 in Participants With Huntington's Disease (HD)". NCT05358717, 2022.
24. Novartis Pharmaceuticals "A Dose Range Finding Study With Open-Label Extension to Evaluate the Safety of Oral LMI070/Branaplam in Early Manifest Huntington's Disease (VIBRANT-HD)". NCT05111249, 2021.
25. Guo Z, Rudow G, Pletnikova O, Codispoti KE, Orr BA, Crain BJ, et al. Striatal neuronal loss correlates with clinical motor impairment in Huntington's disease. Mov Disord. 2012;27(11):1379-86.
26. Mehrabi NF, Waldvogel HJ, Tippett LJ, Hogg VM, Synek BJ, Faull RL. Symptom heterogeneity in Huntington's disease correlates with neuronal degeneration in the cerebral cortex. Neurobiol Dis. 2016;96:67-74.
27. Kim EH, Thu DC, Tippett LJ, Oorschot DE, Hogg VM, Roxburgh R, et al. Cortical interneuron loss and symptom heterogeneity in Huntington disease. Ann Neurol. 2014;75(5):717-27.
28. Thu DC, Oorschot DE, Tippett LJ, Nana AL, Hogg VM, Synek BJ, et al. Cell loss in the motor and cingulate cortex correlates with symptomatology in Huntington's disease. Brain. 2010;133(Pt

4):1094-110.

29. Tippett LJ, Waldvogel HJ, Thomas SJ, Hogg VM, van Roon-Mom W, Synek BJ, et al. Striosomes and mood dysfunction in Huntington's disease. Brain. 2007;130(Pt 1):206-21.
30. Aylward EH, Li Q, Stine OC, Ranen N, Sherr M, Barta PE, et al. Longitudinal change in basal ganglia volume in patients with Huntington's disease. Neurology. 1997;48(2):394-9.
31. Tabrizi SJ, Langbehn DR, Leavitt BR, Roos RA, Durr A, Craufurd D, et al. Biological and clinical manifestations of Huntington's disease in the longitudinal TRACK-HD study: cross-sectional analysis of baseline data. Lancet Neurol. 2009;8(9):791-801.
32. Tabrizi SJ, Reilmann R, Roos RA, Durr A, Leavitt B, Owen G, et al. Potential endpoints for clinical trials in premanifest and early Huntington's disease in the TRACK-HD study: analysis of 24 month observational data. Lancet Neurol. 2012;11(1):42-53.
33. Tabrizi SJ, Scahill RI, Durr A, Roos RA, Leavitt BR, Jones R, et al. Biological and clinical changes in premanifest and early stage Huntington's disease in the TRACK-HD study: the 12-month longitudinal analysis. Lancet Neurol. 2011;10(1):31-42.
34. Tabrizi SJ, Scahill RI, Owen G, Durr A, Leavitt BR, Roos RA, et al. Predictors of phenotypic progression and disease onset in premanifest and early-stage Huntington's disease in the TRACK-HD study: analysis of 36-month observational data. Lancet Neurol. 2013;12(7):637-49.
35. Aylward EH, Brandt J, Codori AM, Mangus RS, Barta PE, Harris GJ. Reduced basal ganglia volume associated with the gene for Huntington's disease in asymptomatic at-risk persons. Neurology. 1994;44(5):823-8.
36. Aylward EH, Codori AM, Barta PE, Pearlson GD, Harris GJ, Brandt J. Basal ganglia volume and proximity to onset in presymptomatic Huntington disease. Arch Neurol. 1996;53(12):1293-6.
37. Paulsen JS, Long JD, Ross CA, Harrington DL, Erwin CJ, Williams JK, et al. Prediction of manifest Huntington's disease with clinical and imaging measures: a prospective observational study. Lancet Neurol. 2014;13(12):1193-201.
38. Scahill RI, Zeun P, Osborne-Crowley K, Johnson EB, Gregory S, Parker C, et al. Biological and clinical characteristics of gene carriers far from predicted onset in the Huntington's disease Young Adult Study (HD-YAS): a cross-sectional analysis. Lancet Neurol. 2020;19(6):502-12.
39. Southwell AL, Smith SE, Davis TR, Caron NS, Villanueva EB, Xie Y, et al. Ultrasensitive measurement of huntingtin protein in cerebrospinal fluid demonstrates increase with Huntington disease stage and decrease following brain huntingtin suppression. Sci Rep. 2015;5:12166.
40. Wild EJ, Boggio R, Langbehn D, Robertson N, Haider S, Miller JR, et al. Quantification of mutant huntingtin protein in cerebrospinal fluid from Huntington's disease patients. J Clin Invest. 2015;125(5):1979-86.
41. Byrne LM, Rodrigues FB, Johnson EB, Wijeratne PA, De Vita E, Alexander DC, et al. Evaluation of mutant huntingtin and neurofilament proteins as potential markers in Huntington's disease. Sci Transl Med. 2018;10(458).

42. Rodrigues FB, Byrne LM, Tortelli R, Johnson EB, Wijeratne PA, Arridge M, et al. Mutant huntingtin and neurofilament light have distinct longitudinal dynamics in Huntington's disease. Sci Transl Med. 2020;12(574).
43. Byrne LM, Rodrigues FB, Blennow K, Durr A, Leavitt BR, Roos RAC, et al. Neurofilament light protein in blood as a potential biomarker of neurodegeneration in Huntington's disease: a retrospective cohort analysis. Lancet Neurol. 2017;16(8):601-9.
44. Constantinescu R, Romer M, Oakes D, Rosengren L, Kieburtz K. Levels of the light subunit of neurofilament triplet protein in cerebrospinal fluid in Huntington's disease. Parkinsonism Relat Disord. 2009;15(3):245-8.
45. Johnson EB, Byrne LM, Gregory S, Rodrigues FB, Blennow K, Durr A, et al. Neurofilament light protein in blood predicts regional atrophy in Huntington disease. Neurology. 2018;90(8):e717-e23.
46. Caron NS, Haqqani AS, Sandhu A, Aly AE, Findlay Black H, Bone JN, et al. Cerebrospinal fluid biomarkers for assessing Huntington disease onset and severity. Brain Commun. 2022;4(6):fcac309.
47. Niemela V, Landtblom AM, Nyholm D, Kneider M, Constantinescu R, Paucar M, et al. Proenkephalin Decreases in Cerebrospinal Fluid with Symptom Progression of Huntington's Disease. Mov Disord. 2021;36(2):481-91.
48. Al Shweiki MR, Oeckl P, Pachollek A, Steinacker P, Barschke P, Halbgebauer S, et al. Cerebrospinal Fluid Levels of Prodynorphin-Derived Peptides are Decreased in Huntington's Disease. Mov Disord. 2021;36(2):492-7.
49. Rodrigues FB, Byrne L, McColgan P, Robertson N, Tabrizi SJ, Leavitt BR, et al. Cerebrospinal fluid total tau concentration predicts clinical phenotype in Huntington's disease. J Neurochem. 2016;139(1):22-5.
50. Constantinescu R, Romer M, Zetterberg H, Rosengren L, Kieburtz K. Increased levels of total tau protein in the cerebrospinal fluid in Huntington's disease. Parkinsonism Relat Disord. 2011;17(9):714-5.
51. Niemela V, Landtblom AM, Blennow K, Sundblom J. Tau or neurofilament light-Which is the more suitable biomarker for Huntington's disease? PLoS One. 2017;12(2):e0172762.
52. Rodrigues FB, Byrne LM, McColgan P, Robertson N, Tabrizi SJ, Zetterberg H, et al. Cerebrospinal Fluid Inflammatory Biomarkers Reflect Clinical Severity in Huntington's Disease. PLoS One. 2016;11(9):e0163479.
53. Niemela V, Burman J, Blennow K, Zetterberg H, Larsson A, Sundblom J. Cerebrospinal fluid sCD27 levels indicate active T cell-mediated inflammation in premanifest Huntington's disease. PLoS One. 2018;13(2):e0193492.
54. Petzold A. Neurofilament phosphoforms: surrogate markers for axonal injury, degeneration and loss. J Neurol Sci. 2005;233(1-2):183-98.
55. Coarelli G, Darios F, Petit E, Dorgham K, Adanyeguh I, Petit E, et al. Plasma neurofilament light chain predicts cerebellar atrophy and clinical progression in spinocerebellar ataxia. Neurobiol Dis.

2021;153:105311.

56. Olsson B, Alberg L, Cullen NC, Michael E, Wahlgren L, Kroksmark AK, et al. NFL is a marker of treatment response in children with SMA treated with nusinersen. J Neurol. 2019;266(9):2129-36.
57. Gaiani A, Martinelli I, Bello L, Querin G, Puthenparampil M, Ruggero S, et al. Diagnostic and Prognostic Biomarkers in Amyotrophic Lateral Sclerosis: Neurofilament Light Chain Levels in Definite Subtypes of Disease. JAMA Neurol. 2017;74(5):525-32.
58. Poesen K, De Schaepdryver M, Stubendorff B, Gille B, Muckova P, Wendler S, et al. Neurofilament markers for ALS correlate with extent of upper and lower motor neuron disease. Neurology. 2017;88(24):2302-9.
59. Lin CH, Li CH, Yang KC, Lin FJ, Wu CC, Chieh JJ, et al. Blood NfL: A biomarker for disease severity and progression in Parkinson disease. Neurology. 2019;93(11):e1104-e11.
60. Mollenhauer B, Dakna M, Kruse N, Galasko D, Foroud T, Zetterberg H, et al. Validation of Serum Neurofilament Light Chain as a Biomarker of Parkinson's Disease Progression. Mov Disord. 2020;35(11):1999-2008.
61. Mattsson N, Andreasson U, Zetterberg H, Blennow K, Alzheimer's Disease Neuroimaging I. Association of Plasma Neurofilament Light With Neurodegeneration in Patients With Alzheimer Disease. JAMA Neurol. 2017;74(5):557-66.
62. Preische O, Schultz SA, Apel A, Kuhle J, Kaeser SA, Barro C, et al. Serum neurofilament dynamics predicts neurodegeneration and clinical progression in presymptomatic Alzheimer's disease. Nat Med. 2019;25(2):277-83.
63. Pawlitzki M, Schreiber S, Bittner D, Kreipe J, Leypoldt F, Rupprecht K, et al. CSF Neurofilament Light Chain Levels in Primary Progressive MS: Signs of Axonal Neurodegeneration. Front Neurol. 2018;9:1037.
64. Disanto G, Barro C, Benkert P, Naegelin Y, Schadelin S, Giardiello A, et al. Serum Neurofilament light: A biomarker of neuronal damage in multiple sclerosis. Ann Neurol. 2017;81(6):857-70.
65. Kuhle J, Nourbakhsh B, Grant D, Morant S, Barro C, Yaldizli O, et al. Serum neurofilament is associated with progression of brain atrophy and disability in early MS. Neurology. 2017;88(9):826-31.
66. Lycke JN, Karlsson JE, Andersen O, Rosengren LE. Neurofilament protein in cerebrospinal fluid: a potential marker of activity in multiple sclerosis. J Neurol Neurosurg Psychiatry. 1998;64(3):402-4.
67. Norgren N, Sundstrom P, Svenningsson A, Rosengren L, Stigbrand T, Gunnarsson M. Neurofilament and glial fibrillary acidic protein in multiple sclerosis. Neurology. 2004;63(9):1586-90.
68. Teunissen CE, Iacobaeus E, Khademi M, Brundin L, Norgren N, Koel-Simmelink MJ, et al. Combination of CSF N-acetylaspartate and neurofilaments in multiple sclerosis. Neurology. 2009;72(15):1322-9.
69. Shahim P, Zetterberg H, Tegner Y, Blennow K. Serum neurofilament light as a biomarker for mild traumatic brain injury in contact sports. Neurology. 2017;88(19):1788-94.

70. Shahim P, Gren M, Liman V, Andreasson U, Norgren N, Tegner Y, et al. Serum neurofilament light protein predicts clinical outcome in traumatic brain injury. Sci Rep. 2016;6:36791.
71. Al Nimer F, Thelin E, Nystrom H, Dring AM, Svenningsson A, Piehl F, et al. Comparative Assessment of the Prognostic Value of Biomarkers in Traumatic Brain Injury Reveals an Independent Role for Serum Levels of Neurofilament Light. PLoS One. 2015;10(7):e0132177.
72. Gisslen M, Price RW, Andreasson U, Norgren N, Nilsson S, Hagberg L, et al. Plasma Concentration of the Neurofilament Light Protein (NFL) is a Biomarker of CNS Injury in HIV Infection: A Cross-Sectional Study. EBioMedicine. 2016;3:135-40.
73. Soylu-Kucharz R, Sandelius A, Sjogren M, Blennow K, Wild EJ, Zetterberg H, et al. Neurofilament light protein in CSF and blood is associated with neurodegeneration and disease severity in Huntington's disease R6/2 mice. Sci Rep. 2017;7(1):14114.
74. Caron NS, Banos R, Yanick C, Aly AE, Byrne LM, Smith ED, et al. Mutant huntingtin is cleared from the brain via active mechanisms in Huntington disease. J Neurosci. 2020.
75. Bondulich MK, Phillips J, Canibano-Pico M, Nita IM, Byrne LM, Wild EJ, et al. Translatable plasma and CSF biomarkers for use in mouse models of Huntington's disease. Brain Commun. 2024;6(1):fcae030.
76. Axelsson M, Malmestrom C, Gunnarsson M, Zetterberg H, Sundstrom P, Lycke J, et al. Immunosuppressive therapy reduces axonal damage in progressive multiple sclerosis. Mult Scler. 2014;20(1):43-50.
77. Gunnarsson M, Malmestrom C, Axelsson M, Sundstrom P, Dahle C, Vrethem M, et al. Axonal damage in relapsing multiple sclerosis is markedly reduced by natalizumab. Ann Neurol. 2011;69(1):83-9.
78. Novakova L, Zetterberg H, Sundstrom P, Axelsson M, Khademi M, Gunnarsson M, et al. Monitoring disease activity in multiple sclerosis using serum neurofilament light protein. Neurology. 2017;89(22):2230-7.
79. Kuhle J, Disanto G, Lorscheider J, Stites T, Chen Y, Dahlke F, et al. Fingolimod and CSF neurofilament light chain levels in relapsing-remitting multiple sclerosis. Neurology. 2015;84(16):1639-43.
80. Novakova L, Axelsson M, Khademi M, Zetterberg H, Blennow K, Malmestrom C, et al. Cerebrospinal fluid biomarkers of inflammation and degeneration as measures of fingolimod efficacy in multiple sclerosis. Mult Scler. 2017;23(1):62-71.
81. Romme Christensen J, Ratzer R, Bornsen L, Lyksborg M, Garde E, Dyrby TB, et al. Natalizumab in progressive MS: results of an open-label, phase 2A, proof-of-concept trial. Neurology. 2014;82(17):1499-507.
82. Winter B, Guenther R, Ludolph AC, Hermann A, Otto M, Wurster CD. Neurofilaments and tau in CSF in an infant with SMA type 1 treated with nusinersen. J Neurol Neurosurg Psychiatry. 2019;90(9):1068-9.
83. Miller TM, Cudkowicz ME, Genge A, Shaw PJ, Sobue G, Bucelli RC, et al. Trial of Antisense Oligonucleotide Tofersen for SOD1 ALS. N Engl J Med. 2022;387(12):1099-110.

84. Hoffmann-La Roche "A Study to Evaluate the Safety, Tolerability, Pharmacokinetics, and Pharmacodynamics of RO7234292 (ISIS 443139) in Huntington's Disease Patients Who Participated in Prior Investigational Studies of RO7234292 (ISIS 443139)". NCT03342053, 2018.
85. Tabrizi SJ, Leavitt BR, Landwehrmeyer GB, Wild EJ, Saft C, Barker RA, et al. Targeting Huntingtin Expression in Patients with Huntington's Disease. N Engl J Med. 2019;380(24):2307-16.
86. McColgan P, Thobhani A, Boak L, Schobel SA, Nicotra A, Palermo G, et al. Tominersen in Adults with Manifest Huntington's Disease. N Engl J Med. 2023;389(23):2203-5.
87. Slow EJ, van Raamsdonk J, Rogers D, Coleman SH, Graham RK, Deng Y, et al. Selective striatal neuronal loss in a YAC128 mouse model of Huntington disease. Hum Mol Genet. 2003;12(13):1555-67.
88. Petrella LI, Castelhano JM, Ribeiro M, Sereno JV, Goncalves SI, Laco MN, et al. A whole brain longitudinal study in the YAC128 mouse model of Huntington's disease shows distinct trajectories of neurochemical, structural connectivity and volumetric changes. Hum Mol Genet. 2018;27(12):2125-37.
89. Carroll JB, Lerch JP, Franciosi S, Spreeuw A, Bissada N, Henkelman RM, et al. Natural history of disease in the YAC128 mouse reveals a discrete signature of pathology in Huntington disease. Neurobiol Dis. 2011;43(1):257-65.
90. Van Raamsdonk JM, Pearson J, Slow EJ, Hossain SM, Leavitt BR, Hayden MR. Cognitive dysfunction precedes neuropathology and motor abnormalities in the YAC128 mouse model of Huntington's disease. J Neurosci. 2005;25(16):4169-80.
91. Pouladi MA, Stanek LM, Xie Y, Franciosi S, Southwell AL, Deng Y, et al. Marked differences in neurochemistry and aggregates despite similar behavioural and neuropathological features of Huntington disease in the full-length BACHD and YAC128 mice. Hum Mol Genet. 2012;21(10):2219-32.
92. Brooks S, Higgs G, Janghra N, Jones L, Dunnett SB. Longitudinal analysis of the behavioural phenotype in YAC128 (C57BL/6J) Huntington's disease transgenic mice. Brain Res Bull. 2012;88(2-3):113-20.
93. Van Raamsdonk JM, Pearson J, Murphy Z, Hayden MR, Leavitt BR. Wild-type huntingtin ameliorates striatal neuronal atrophy but does not prevent other abnormalities in the YAC128 mouse model of Huntington disease. BMC Neurosci. 2006;7:80.
94. Caron NS, Anderson C, Black HF, Sanders SS, Lemarie FL, Doty CN, et al. Reliable Resolution of Full-Length Huntingtin Alleles by Quantitative Immunoblotting. J Huntingtons Dis. 2021.
95. Reindl W, Baldo B, Schulz J, Janack I, Lindner I, Kleinschmidt M, et al. Meso scale discovery-based assays for the detection of aggregated huntingtin. PLoS One. 2019;14(3):e0213521.
96. R Core Team. R: A language and environment for statistical computing. R Foundation for Statistical Computing, Vienna, Austria. https://www.R-project.org/. 2020.
97. Bates D, Mächler M, Bolker B, Walker S. Fitting Linear Mixed-Effects Models Using lme4. Journal of Statistical Software. 2015;67(1):1 - 48.

98. Boegman RJ, el-Defrawy SR, Jhamandas K, Beninger RJ, Ludwin SK. Quinolinic acid neurotoxicity in the nucleus basalis antagonized by kynurenic acid. Neurobiol Aging. 1985;6(4):331-6.
99. Caron NS, Banos R, Aly AE, Xie Y, Ko S, Potluri N, et al. Cerebrospinal fluid mutant huntingtin is a biomarker for huntingtin lowering in the striatum of Huntington disease mice. Neurobiol Dis. 2022;166:105652.
100. DiFiglia M, Sapp E, Chase KO, Davies SW, Bates GP, Vonsattel JP, et al. Aggregation of huntingtin in neuronal intranuclear inclusions and dystrophic neurites in brain. Science. 1997;277(5334):1990-3.
101. Khalil M, Pirpamer L, Hofer E, Voortman MM, Barro C, Leppert D, et al. Serum neurofilament light levels in normal aging and their association with morphologic brain changes. Nat Commun. 2020;11(1):812.
102. Iliff JJ, Wang M, Liao Y, Plogg BA, Peng W, Gundersen GA, et al. A paravascular pathway facilitates CSF flow through the brain parenchyma and the clearance of interstitial solutes, including amyloid beta. Sci Transl Med. 2012;4(147):147ra11.
103. Schwarcz R, Whetsell WO, Jr., Mangano RM. Quinolinic acid: an endogenous metabolite that produces axon-sparing lesions in rat brain. Science. 1983;219(4582):316-8.
104. Finkel RS, Mercuri E, Darras BT, Connolly AM, Kuntz NL, Kirschner J, et al. Nusinersen versus Sham Control in Infantile-Onset Spinal Muscular Atrophy. N Engl J Med. 2017;377(18):1723-32.
105. Mortberg MA, Gentile JE, Nadaf NM, Vanderburg C, Simmons S, Dubinsky D, et al. A single-cell map of antisense oligonucleotide activity in the brain. Nucleic Acids Res. 2023;51(14):7109-24.
106. Caron NS, Aly AE, Black HF, Martin DDO, Schmidt ME, Ko S, et al. Systemic delivery of mutant huntingtin lowering antisense oligonucleotides to the brain using apolipoprotein A-I nanodisks for Huntington disease. J Control Release. 2024.
107. Wu TT, Su FJ, Feng YQ, Liu B, Li MY, Liang FY, et al. Mesenchymal stem cells alleviate AQP-4-dependent glymphatic dysfunction and improve brain distribution of antisense oligonucleotides in BACHD mice. Stem Cells. 2020;38(2):218-30.
108. Nedergaard M, Goldman SA. Glymphatic failure as a final common pathway to dementia. Science. 2020;370(6512):50-6.
109. Kress BT, Iliff JJ, Xia M, Wang M, Wei HS, Zeppenfeld D, et al. Impairment of paravascular clearance pathways in the aging brain. Ann Neurol. 2014;76(6):845-61.
110. Zhou Y, Cai J, Zhang W, Gong X, Yan S, Zhang K, et al. Impairment of the Glymphatic Pathway and Putative Meningeal Lymphatic Vessels in the Aging Human. Ann Neurol. 2020;87(3):357-69.
111. Stanek LM, Sardi SP, Mastis B, Richards AR, Treleaven CM, Taksir T, et al. Silencing mutant huntingtin by adeno-associated virus-mediated RNA interference ameliorates disease manifestations in the YAC128 mouse model of Huntington's disease. Hum Gene Ther. 2014;25(5):461-74.
112. Kotowska-Zimmer A, Przybyl L, Pewinska M, Suszynska-Zajczyk J, Wronka D, Figiel M, et al. A CAG repeat-targeting artificial miRNA lowers the mutant huntingtin level in the YAC128 model of Huntington's disease. Mol Ther Nucleic Acids. 2022;28:702-15.

113. Miniarikova J, Zimmer V, Martier R, Brouwers CC, Pythoud C, Richetin K, et al. AAV5-miHTT gene therapy demonstrates suppression of mutant huntingtin aggregation and neuronal dysfunction in a rat model of Huntington's disease. Gene Ther. 2017;24(10):630-9.

114. Southwell AL, Skotte NH, Kordasiewicz HB, Ostergaard ME, Watt AT, Carroll JB, et al. In vivo evaluation of candidate allele-specific mutant huntingtin gene silencing antisense oligonucleotides. Mol Ther. 2014;22(12):2093-106.

Figures

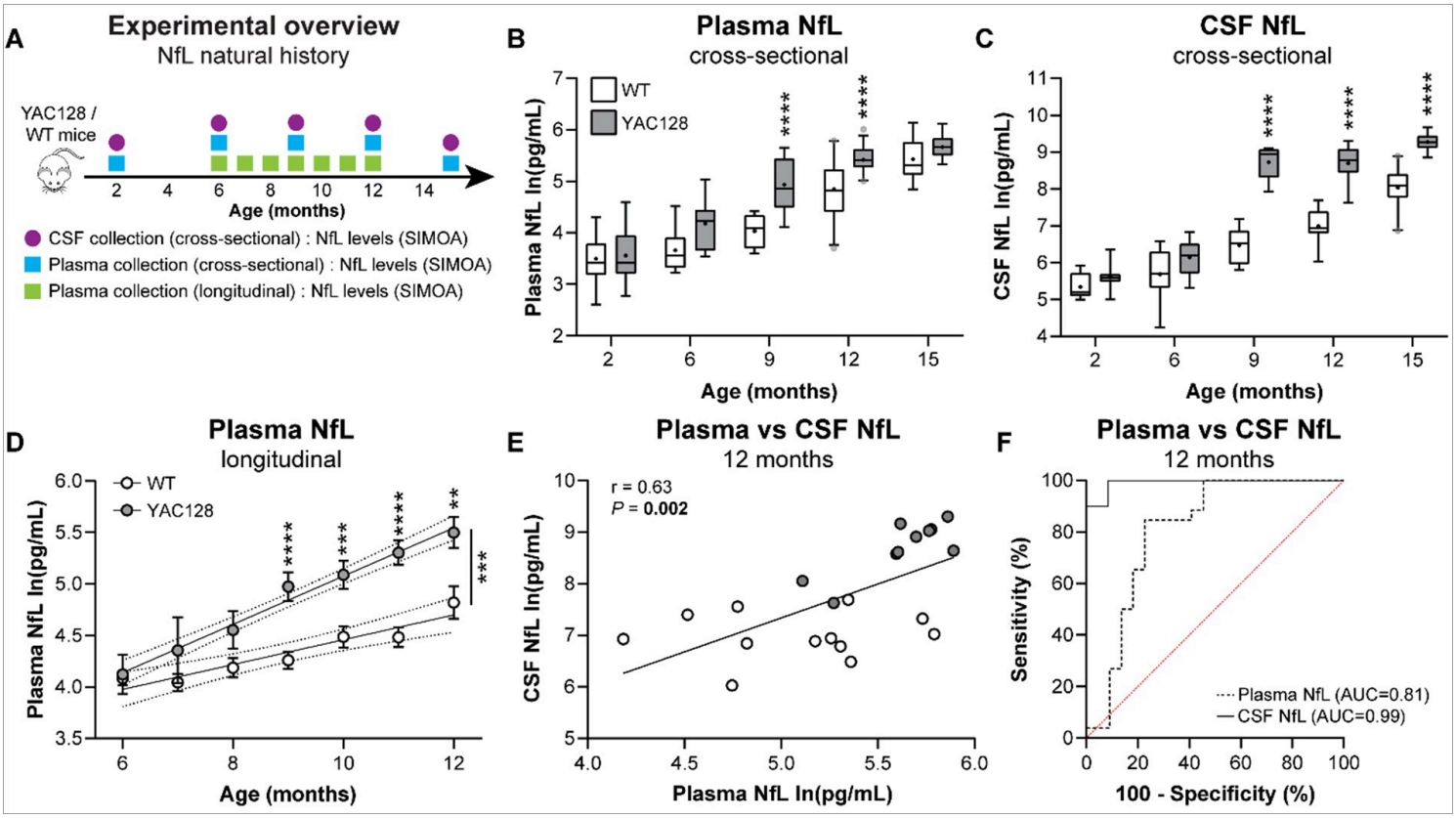


Figure 1

Plasma and CSF NfL are elevated over the natural history of disease in YAC128 mice. (**A**) Schematic diagram of experimental design. Cross-sectional NfL concentrations (natural log pg/mL) in (**B**) plasma (N = 8-26 animals/genotype/age. Two-way ANOVA: genotype $P < 0.0001$, age $P < 0.0001$, interaction $P = 0.008$. ****$P < 0.0001$) and (**C**) CSF from YAC128 and WT littermate control mice (N = 6-20 animals/genotype/age. Two-way ANOVA: genotype $P < 0.0001$, age $P < 0.0001$, interaction $P < 0.0001$. ****$P < 0.0001$). (**D**) Longitudinal plasma NfL concentrations from 6 to 12 months of age in WT and YAC128 mice (N = 18-21 animals/genotype/age. Mixed-effect analysis: genotype $P < 0.0001$, age $P < 0.0001$, genotype x age $P < 0.0001$. **$P = 0.005$, ***$P = 0.0002$, ****$P < 0.0001$. Linear regression: WT: Y = 0.1205X + 3.254, $R^2 = 0.90$, $P = 0.001$. YAC128: Y = 0.2341X + 2.735, $R^2 = 0.99$, $P < 0.0001$. Comparison of slopes: ***$P = 0.0005$). Dashed lines represent 95% confidence bands of the best fit lines. (**E**) Correlation of NfL concentrations between paired plasma and CSF samples from WT (white circles) and

YAC128 mice (grey circles) at 12 months of age (N = 10-12 animals/genotype/biofluid. Pearson's correlation: r = 0.63, *P* = 0.0018). (**F**) ROC curve comparing sensitivity and specificity of plasma NfL (AUC = 0.81, *P* = 0.0003) and CSF NfL (N = 10-12 animals/genotype/biofluid. AUC = 0.99, *P* = 0.0001) for discriminating between YAC128 and WT mice at 12 months of age. Plasma and CSF NfL concentrations are natural log transformed.

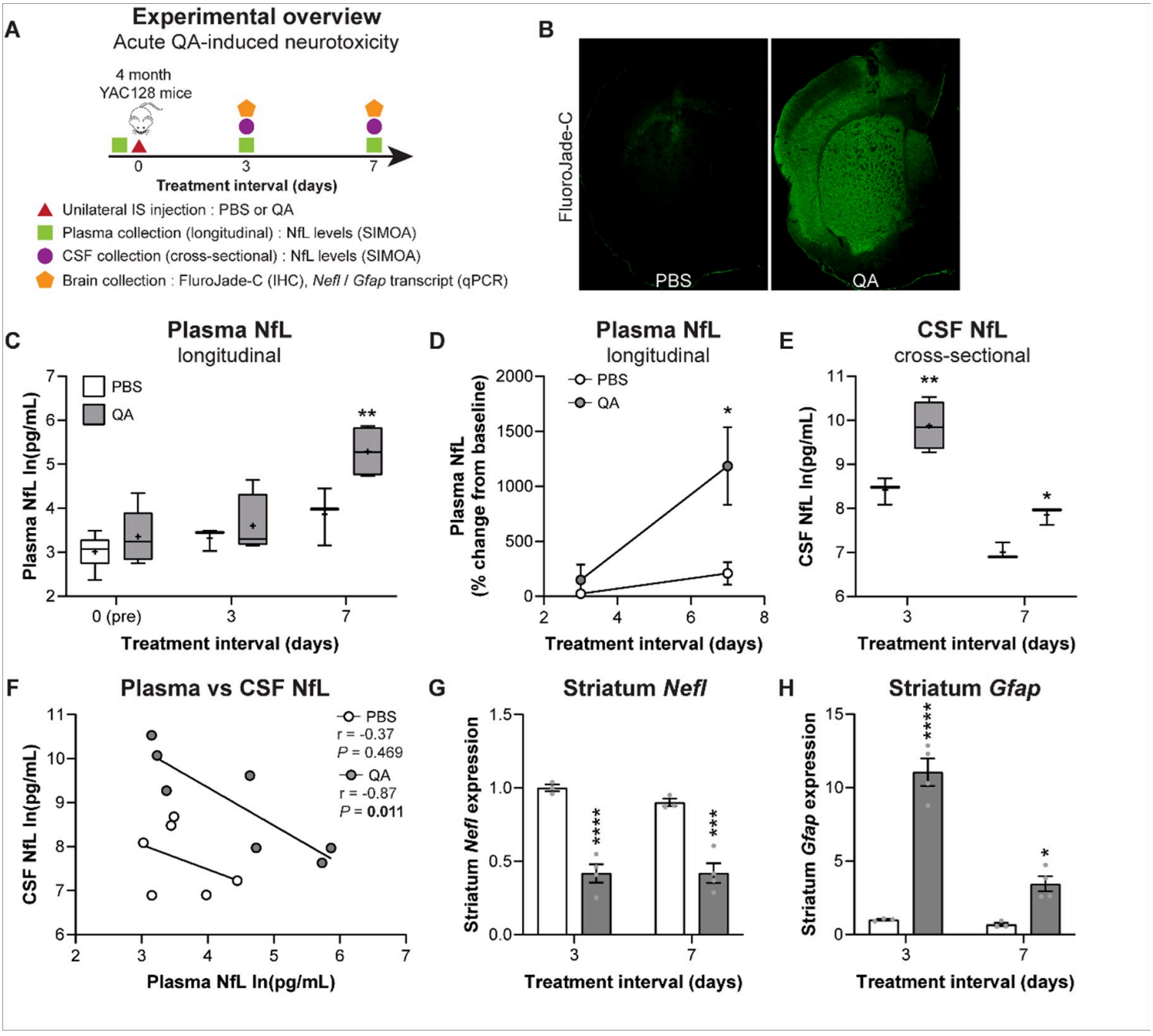


Figure 2

Acute neurodegeneration in the striatum of YAC128 mice leads to increased plasma and CSF NfL concentrations. (**A**) Schematic diagram of experimental design (N = 3-4 animals/condition/timepoint). (**B**) IHC images of Fluoro-Jade C staining in YAC128 mice injected with either PBS or QA at 3 days post-injection. (**C**) Longitudinal plasma NfL concentrations at baseline and 3- and 7-days after injection with

either PBS or QA (Two-way ANOVA: treatment $P = 0.005$, interval $P < 0.0001$, interaction $P = 0.093$. $^{**}P = 0.007$). (**D**) Percent change of plasma NfL concentrations from baseline following at 3- and 7-days post-injection of PBS (white circles) or QA (grey circles) (Two-way ANOVA: treatment $P = 0.037$, interval $P = 0.024$, interaction $P = 0.093$. $^{*}P = 0.026$). (**E**) Cross-sectional CSF concentrations at 3 and 7 days after treatment with either PBS or QA (Two-way ANOVA: treatment $P = 0.0003$, interval $P < 0.0001$, interaction $P = 0.176$. $^{*}P = 0.040$, $^{**}P = 0.001$). (**F**) Correlation of NfL concentrations between paired plasma and CSF samples at 3- and 7-days post-injection with PBS (white circles; r = -0.37, $P = 0.469$) or QA (grey circles; r = -0.87, $P = 0.011$). Relative expression of (**G**) *Nefl* (Two-way ANOVA: treatment $P < 0.0001$, interval $P = 0.403$, interaction $P = 0.394$. $^{***}P = 0.0003$, $^{****}P < 0.0001$) and (**H**) *Gfap* in the injected striatum following unilateral IS injections of either PBS or QA (Two-way ANOVA: treatment $P < 0.0001$, interval $P < 0.0001$, interaction $P = 0.0002$. $^{*}P = 0.024$, $^{****}P < 0.0001$). Fold changes are presented relative to PBS values at 3 days post-QA injection. Plasma and CSF NfL values are natural log transformed.

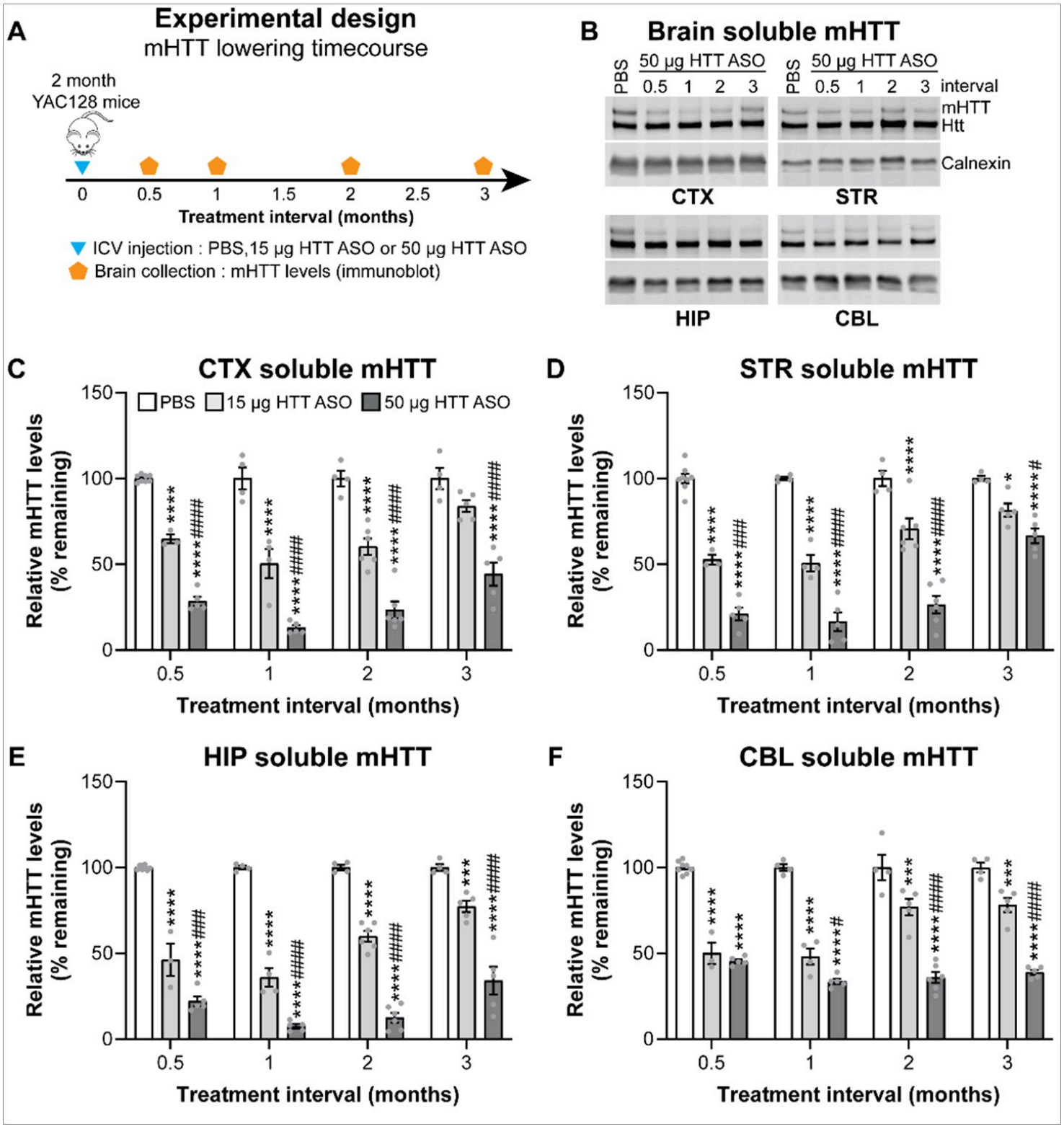


Figure 3

Sustained, dose-dependent lowering of mHTT in the brain of YAC128 mice with a HTT ASO. (**A**) Schematic diagram of experimental design (N = 3-8 animals/condition/timepoint). (**B**) Representative immunoblots and quantification of relative soluble mHTT levels in the (**C**) cortex (Two-way ANOVA: treatment P <0.0001, timepoint P < 0.0001, interaction P = 0.0319. HTT ASO compared to PBS: ****P < 0.0001. 50 µg compared to 15 µg HTT ASO: $^{\#\#\#\#}P$ < 0.0001), (**D**) striatum (Two-way ANOVA: treatment P

< 0.0001, timepoint $P < 0.0001$, interaction $P < 0.0001$. HTT ASO compared to PBS: *$P = 0.018$, ****$P < 0.0001$. 50 µg compared to 15 µg HTT ASO: $^{\#}P = 0.046$, $^{\#\#\#}P = 0.0001$, $^{\#\#\#\#}P < 0.0001$), (**E**) hippocampus (Two-way ANOVA: treatment $P < 0.0001$, timepoint $P < 0.0001$, interaction $P < 0.0001$. HTT ASO compared to PBS: ***$P = 0.0005$, ****$P < 0.0001$. 50 µg compared to 15 µg HTT ASO: $^{\#\#\#}P = 0.0007$, $^{\#\#\#\#}P < 0.0001$), and (**F**) cerebellum (Two-way ANOVA: treatment $P < 0.0001$, timepoint $P = 0.0006$, interaction $P < 0.0001$. HTT ASO compared to PBS: ***$P = 0.0001$, ****$P < 0.0001$. 50 µg compared to 15 µg HTT ASO: $^{\#}P = 0.017$, $^{\#\#\#\#}P < 0.0001$) from YAC128 mice treated at 2 months of age with either PBS, 15 µg HTT ASO or 50 µg HTT ASO. All mHTT target engagement data are shown relative to values from PBS at the 0.5-month interval.

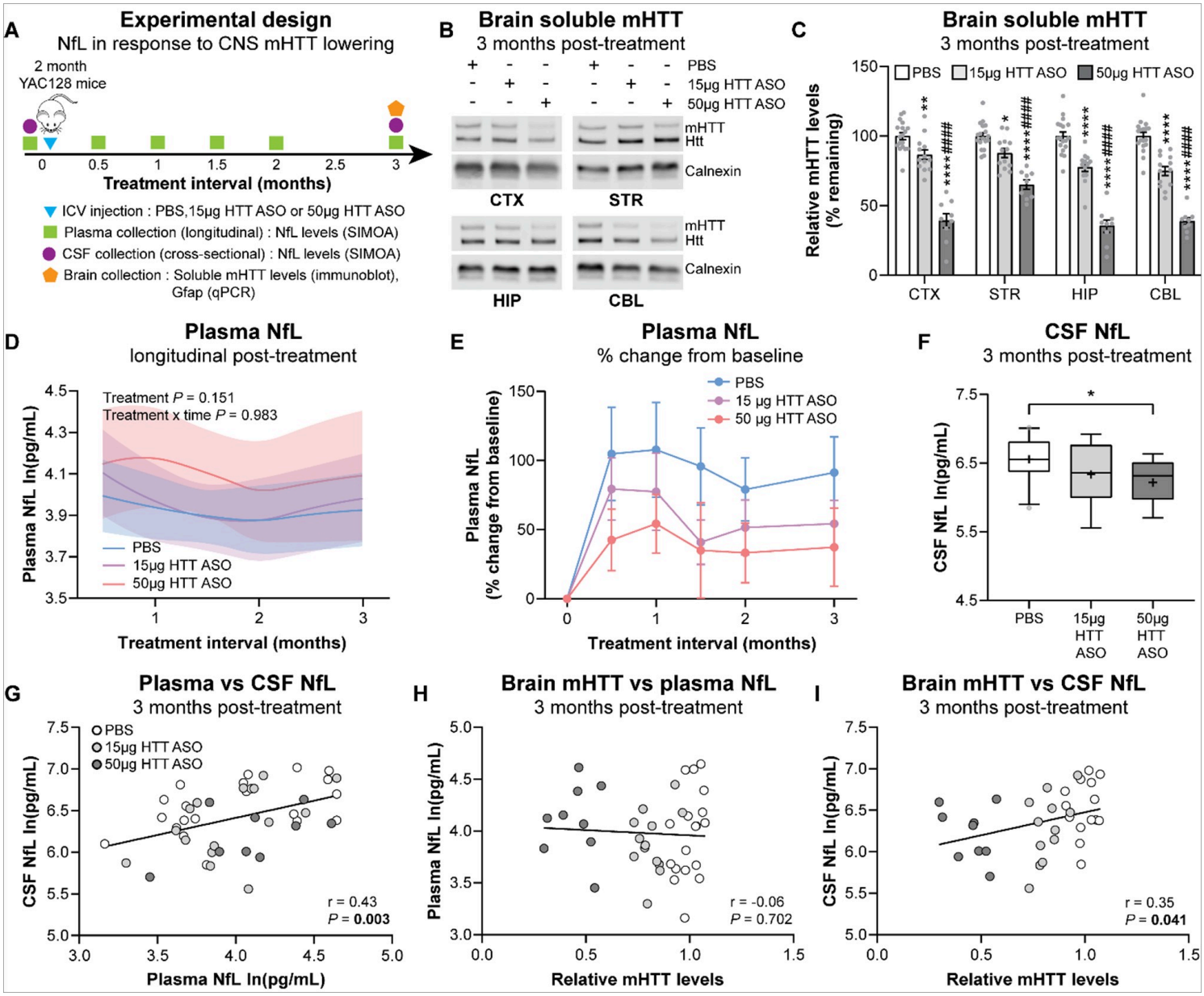


Figure 4

Lowering mHTT in the brain of YAC128 mice prior to motor deficits and regional forebrain atrophy leads to a reduction of CSF NfL concentrations. (**A**) Schematic diagram of experimental design (N = 9-18

animals/condition). (**B**) Representative immunoblots and (**C**) quantification of relative soluble mHTT levels in the CTX, STR, HIP and CBL of YAC128 mice treated at 2 months of age with either PBS, 15 µg or 50 µg HTT ASO and assessed 3 months post-treatment at 5 months of age (Two-way ANOVA: treatment $P < 0.0001$, brain region $P < 0.0001$, interaction $P = 0.0001$. HTT ASO compared to PBS: *$P = 0.013$, **$P = 0.006$, ****p<0.0001. 50 µg compared to 15 µg HTT ASO: $^{###}P = 0.0007$, $^{####}P < 0.0001$). (**D**) Longitudinal plasma NfL concentrations following treatment of YAC128 mice with either PBS, 15 µg HTT ASO or 50 µg HTT ASO (Linear mixed-effects model: treatment $P = 0.151$, treatment x time interaction $P = 0.983$). (**E**) Percent change in longitudinal plasma NfL concentrations from baseline at different intervals following treatment with either PBS, 15 µg HTT ASO or 50 µg HTT ASO (Mixed-effects model: treatment $P = 0.190$, time $P = 0.396$, treatment x time $P = 0.998$). (**F**) Cross-sectional CSF NfL concentrations at 3 months post-treatment with either PBS, 15 µg or 50 µg HTT ASO (One-way ANOVA: $P = 0.032$. *$P = 0.044$. Linear regression: $Y = -0.0068X + 6.520$, $R^2 = 0.12$, $P = 0.0161$). (**G**) Correlation of NfL concentrations between paired plasma and CSF samples from YAC128 mice treated with PBS, 15 µg or 50 µg HTT ASO (Pearson's correlation: r = 0.43, $P = 0.003$). Correlation of relative mHTT levels in the whole brain (mean mHTT from all brain regions for each animal) and either (**H**) plasma NfL (Pearson's correlation: r = -0.06, $P = 0.702$) or (**I**) CSF NfL (Pearson's correlation: r = 0.35, $P = 0.041$) from the same animal at 3 months post-treatment with PBS, 15 µg or 50 µg HTT ASO. Plasma and CSF NfL values are natural log transformed.

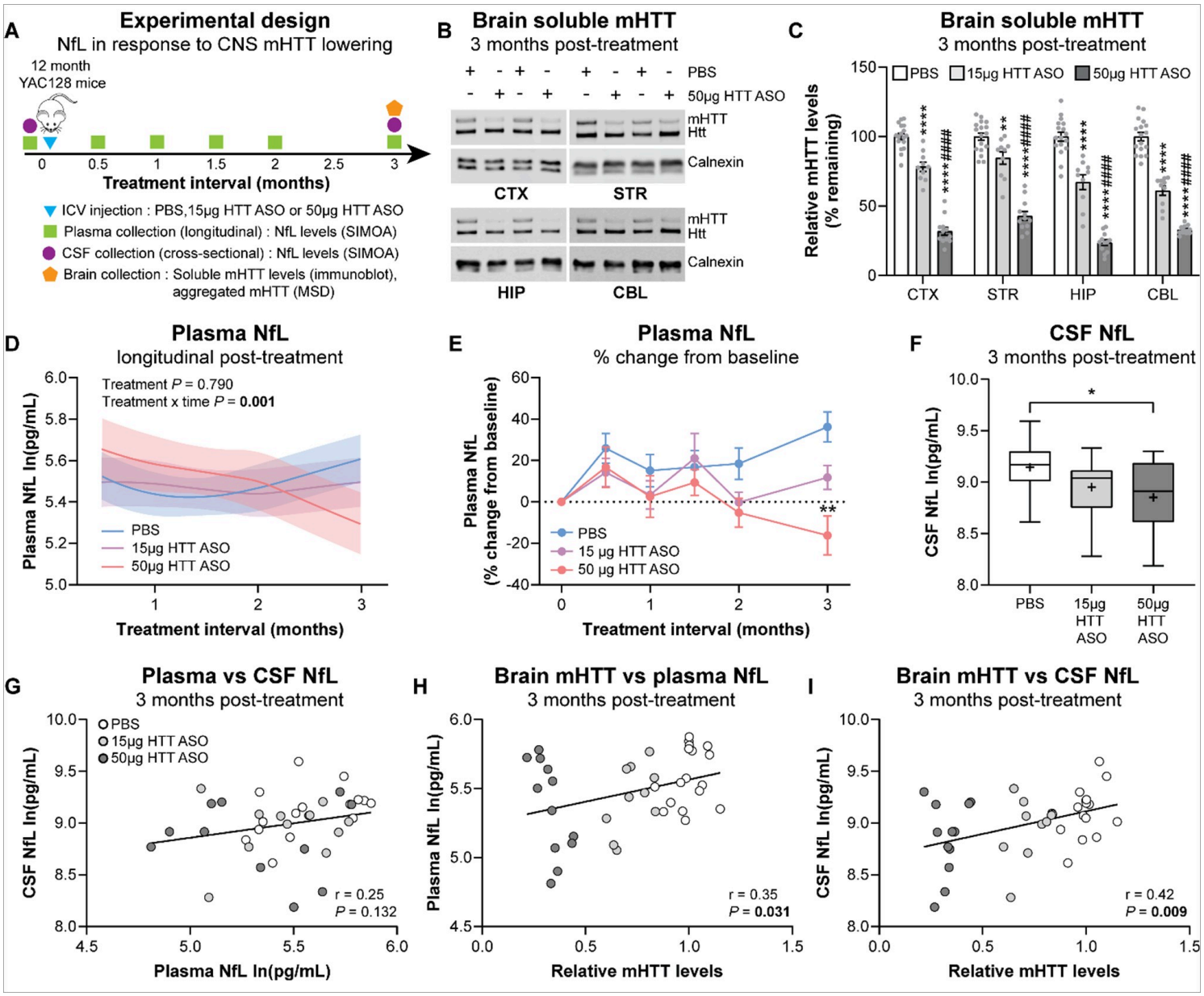


Figure 5

Plasma and CSF NfL concentrations are stabilized in response to mHTT lowering in the brain initiated after onset of striatal neuron loss in YAC128 mice. (**A**) Schematic diagram of experimental design (N = 10-17 animals/condition). (**B**) Representative immunoblots and (**C**) quantification of relative soluble mHTT levels in the CTX, STR, HIP and CBL of YAC128 mice treated at 12 months of age with either PBS, 15 µg or 50 µg HTT ASO and assessed 3 months post-treatment at 15 months of age (Two-way ANOVA: treatment $P < 0.0001$, brain region $P < 0.0001$, interaction $P = 0.0009$. HTT ASO compared to PBS: $^{**}P = 0.002$, ****p<0.0001. 50 µg compared to 15 µg HTT ASO: $^{\#\#\#\#}P < 0.0001$). (**D**) Longitudinal plasma NfL concentrations following treatment of YAC128 mice with either PBS, 15 µg or 50 µg HTT ASO (Linear mixed-effects model: treatment $P = 0.790$, treatment x time interaction $P = 0.001$). (**E**) Percent change in longitudinal plasma NfL concentrations from baseline at different intervals following treatment with either PBS, 15 µg or 50 µg HTT ASO (Mixed-effects model: treatment $P = 0.057$, time $P = 0.039$, treatment x time $P = 0.015$. $^{**}P = 0.003$). **F**) Cross-sectional CSF NfL concentrations at 3 months post-treatment

with either PBS, 15 µg or 50 µg HTT ASO (One-way ANOVA: $P = 0.025$. *$P = 0.024$. Linear regression: Y = -0.0057X + 9.117, $R^2 = 0.16$, $P = 0.011$). (**G**) Correlation of NfL concentrations between paired plasma and CSF samples from YAC128 mice treated with PBS, 15 µg or 50 µg HTT ASO (Pearson's correlation: r = 0.25, $P = 0.132$). Correlation of relative mHTT levels in the whole brain (mean mHTT from all brain regions for each animal) and either (**H**) plasma NfL (Pearson's correlation: r = 0.35, $P = 0.031$) or (**I**) CSF NfL (Pearson's correlation: r = 0.42, $P = 0.009$) from the same animal at 3 months post-treatment with PBS, 15 µg or 50 µg HTT ASO. Plasma and CSF NfL values are natural log transformed.

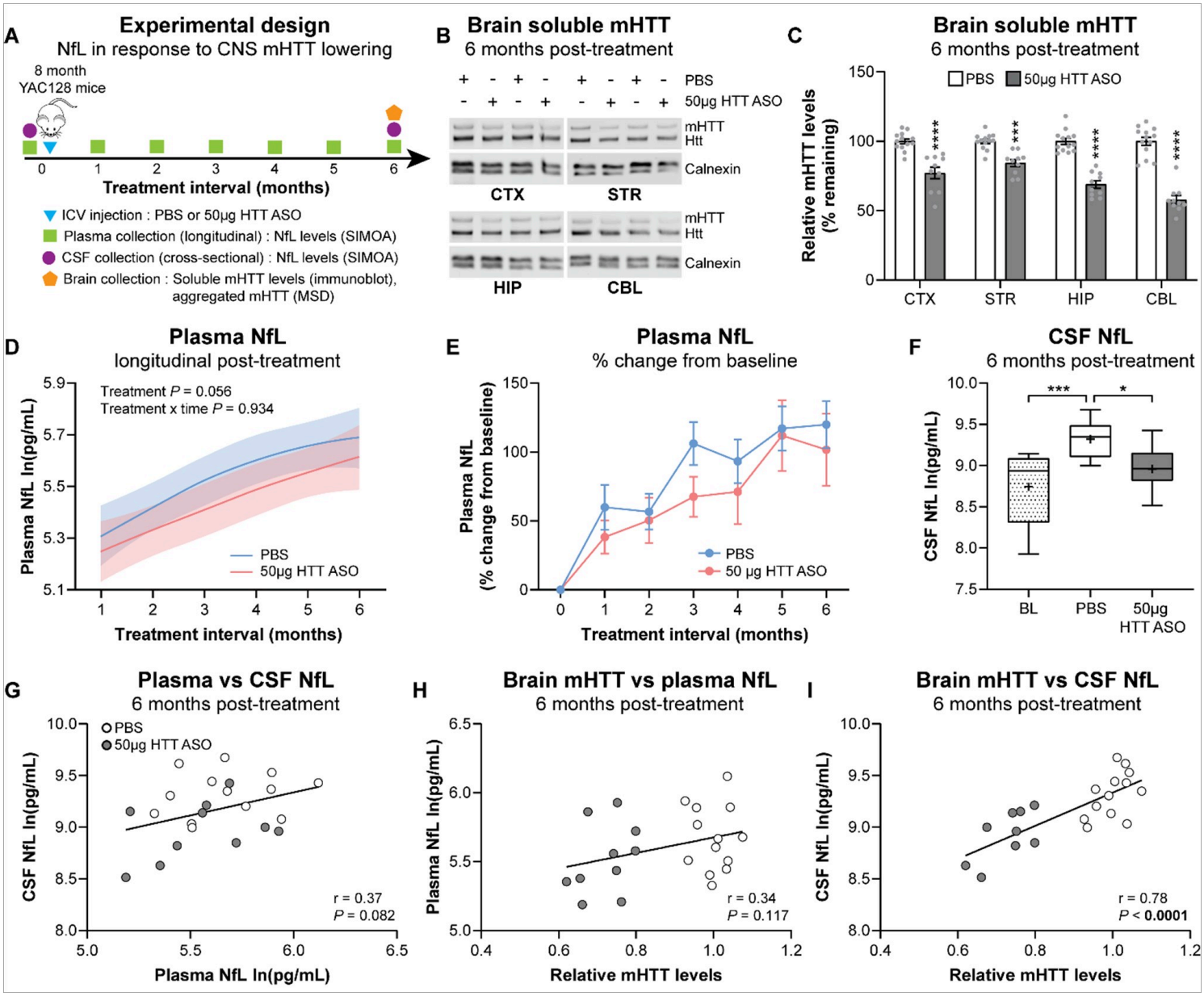


Figure 6

Sustained reduction of mHTT in the brain of YAC128 mice initiated prior to overt striatal neuron loss stabilizes increase of plasma and CSF NfL. (**A**) Schematic diagram of experimental design (N = 10-13 animals/condition). (**B**) Representative immunoblots and (**C**) quantification of relative soluble mHTT levels in the CTX, STR, HIP and CBL of YAC128 mice treated at 8 months of age with either PBS or 50 µg HTT ASO and assessed 6 months post-treatment at 14 months of age (Two-way ANOVA: treatment $P <$

0.0001, brain region $P < 0.0001$, interaction $P < 0.0001$. ***$P = 0.0003$, ****$P < 0.0001$). (**D**) Longitudinal plasma NfL concentrations following treatment of YAC128 mice with either PBS or 50 µg HTT ASO (Linear mixed-effects model: treatment $P = 0.056$, treatment x time interaction $P = 0.934$). (**E**) Percent change in longitudinal plasma NfL concentrations from baseline at different intervals following treatment with either PBS or 50 µg HTT ASO (Mixed-effects model: treatment $P = 0.411$, time $P < 0.0001$, treatment x time $P = 0.565$). (**F**) Cross-sectional CSF NfL concentrations at baseline (8 months) and 6 months post-treatment with either PBS or 50 µg HTT ASO (One-way ANOVA: $P = 0.0007$. PBS compared to baseline: ***$P = 0.0007$; 50 µg HTT ASO compared to PBS: *$P = 0.020$). (**G**) Correlation of NfL concentrations between paired plasma and CSF samples from YAC128 mice treated with PBS or 50 µg HTT ASO (Pearson's correlation: r = 0.37, $P = 0.082$). Correlation of relative mHTT levels in the whole brain (mean mHTT from all brain regions for each animal) and either (**H**) plasma NfL (Pearson's correlation: r = 0.34, $P = 0.117$) or (**I**) CSF NfL (Pearson's correlation: r = 0.78, $P < 0.0001$) from the same animal at 6 months post-treatment with PBS or 50 µg HTT ASO. Plasma and CSF NfL values are natural log transformed.

Supplementary Files

This is a list of supplementary files associated with this preprint. Click to download.

- NFLmHTTloweringAdditionalfile1TranslNeurodegener.docx